

Experimental Investigations on the Mechanical Properties and Microstructure of Al7075-TiN Nano-Composite Formed by Friction Stir Processing

Reza Hashemi

Submitted to the
Institute of Graduate Studies and Research
in partial fulfillment of the requirements for the Degree of

Master of Science
in
Mechanical Engineering

Eastern Mediterranean University
February 2014
Gazimağusa, North Cyprus

Approval of Institute of Graduate Studies and Research

Prof. Dr. Elvan Yilmaz
Director

I certify that this thesis satisfies the requirements as thesis for degree of Master of Science in Mechanical Engineering.

Prof. Dr. Uğur Atıkol
Chair, Department of Mechanical Engineering

We certify that we have read this thesis and that is our opinion it is fully adapted in scope and quality as a thesis for the degree of Master of Science in Mechanical Engineering.

Asst. Prof. Dr. Ghulam Hussain
Supervisor

Examining Committee

1. Assoc. Prof. Dr. Hasan Hacısevki

2. Asst. Prof. Dr. Ghulam Hussain

3. Asst. Prof. Dr. Mostafa Ranjbar

ABSTRACT

Friction stir processing (FSP), originally based on friction stir welding, is believed to be a cost-effective solid state mechanical alloying technique very useful to produce composites. This makes use of a simple mechanical tool stirring and mixing material in localized region to cause dynamic recrystallization to produce new microstructures. In this study, FSP was applied to produce AL-TiN nano-composite with 7075-T6 aluminium as matrix phase. Three major parameters of the process, namely tool geometry, number of passes and tool rotation direction, were varied to realize the composite while the other parameters as penetration, tilt angle feed rate and rotational speed were kept fixed. In order to characterize the newly formed composite, various tests including optical microscope, SEM, EDS, XRD, micro-hardness, tension and wear tests (pin on disc) were performed in the FSP zone. The results showed that the FSP process produced TiN based composite of nano-size with various phases. The distribution of nano-particles was found to be dependent on the process parameters. The distribution of particles was tend to become uniform with increasing passes, alternative changing of tool rotation and threaded tapered tool. The grain size reduced significantly and followed the aforesaid trend in respect of effect of parameters. With particles distributed more evenly, the average hardness was found to be increasing. Further, the hardness was higher than the matrix material. However, ductility most probably due to presence of intermetallics in the composite reduced and the same was found to be true for tensile strength. The wear tests showed remarkable improvement in the wear performance of matrix material after processing with FSP (i.e., composite).

The current study has shown that FSP can be employed as a useful tool to produce low-cost nano-composites with improved wear and mechanical properties satisfying the needs of modern engineering. Furthermore, this study will act as a guideline to the materials engineers to produce required materials with modifies properties.

Keywords:Friction Stir Processing, Mechanical properties, Microstructure, Xrd, SEM, Hardness, Tensile, Wear, Nano-powder, composite, TiN, Al 7075

ÖZ

Sürtünme karıştırma işleme (FSP), başlangıçta sürtünme karıştırma kaynakdayalı, kompozit üretmek için çok yararlı bir maliyeti-düşük bir katı hal mekanik alaşımlama tekniği olduğuna inanılmaktadır. Bu yeni mikroyapılarının oluşturulması için Dinamik yeniden kristalleştirmenin harekete neden olmak için lokalize bir bölgede bulunan bir malzeme karıştırma ve basit bir mekanik araç kullanır. Bu çalışmada, FSP matris faz olarak 7075-T6 alüminyumdan ile AL-TiN nano-kompoziti üretmek için uygulanmıştır. Sürecin üç önemli parametre, yani takım geometrisi, geçiş ve takım dönüş yönü sayısı, penetrasyonu gibi diğer parametreler, eğim açısı besleme hızı ve dönüş hızı, sabit tutuldu ise bileşik gerçekleştirmek için değiştirildi. FSP bölgesinde, yeni oluşturulan kompozit bölgesinde, Optik mikroskop, SEM, EDS, XRD, mikro-sertlik, gerginlik ve testler aşınma (diskte pin) dahil olmak üzere, çeşitli testler karakterize etmek amacıyla yapıldı. Sonuçlar, FSP, çeşitli işlem aşamaları ile nano boyutta TiN göre bileşik ürettiğini göstermiştir. Nano-partiküllerin dağılımı proses parametrelerine bağlı olarak bulunmuştur. Parçacıkların dağılımı, artan paslar ile uniform olma eğilimi edildi, aracı dönme ve dişli konik aracı alternatif değişiyor. Tane boyutunu önemli ölçüde azaltmıştır ve parametrelerin etkisi ile ilgili olarak daha önce bahsedilen eğilim izledi. Daha eşit dağılmış partiküller ile, ortalama bir sertlik arttığı bulunmuştur. Ayrıca, sertlik matris malzemesi daha yüksekti. Ancak, Dactility muhtemelen azaltılmış bileşik ve aynı ntermetaliklerin varlığı süneklik çekme Aşınma testleri, FSP ile işlendikten sonra matris malzemesinin aşınma performansında kayda değer bir iyileşme gösterdi. Bu çalışma, FSP geliştirilmiş aşınma ve modern mühendislik ihtiyaçlarına cevap, mekanik özelliklere sahip düşük maliyetli nano-kompozitler üretmek için yararlı bir araç

olarak kullanılabilir göstermiştir. Ayrıca, bu çalışmanın sonuçları gerekli malzemeleri üretmek için malzeme mühendislerine bir kılavuz olarak hareket edecektir.

Anahtar Kelimeler: Sürtünme karıştırma işleme, Mekanik özellikler, Mikroyapı, Xrd, SEM, Sertlik, Çekme, Nano-toz, kompozit TiN, Al7075, Sürtünme

TO MY FAMILY

ACKNOWLEDGMENT

The completion of this work is due to the support and guidance of many people. First, I would like to express my sincere appreciation and gratitude to my supervisor, Assist. Prof. DrGhulamHussainfor his support, guidance, enthusiasm and encouragements throughout mystudies and research progress.

I would like to thank all my friends AliZarif, Mahmoud Shahbaznia, Seed Ayaziyan, PayamAlikhani, because of their invaluable support to this work. Also I would like to acknowledge the collaboration of Engineering College of Tehran University and METU engineering labs.

My deepest appreciation goes to my parents for their emotional, moral and financial supports. Also, I would like to thanks my brothers for providing motivation and encouragement and guideline as a role model in my academic life.

TABLE OF CONTENT

ABSTRACT	iii
ÖZ	v
DEDICATION.....	vii
ACKNOWLEDGMENT	viii
LIST OF FIGURES	xiii
LIST OF SYMBOLS	xvi
1 INTRODUCTION	1
1.1 Aluminium	1
1.1.1 Types of Wrought Aluminium.....	1
1.1.1.1 1xxx Alloy Series	1
1.1.1.2 2xxx Alloy Series	1
1.1.1.3 3xxx Alloy Series	2
1.1.1.4 4xxx Alloy Series	2
1.1.1.5 5xxx Alloy Series	2
1.1.1.6 6xxx Alloy Series	2
1.1.1.7 7xxx Alloy Series	3
1.2 Definition of the Problem	5
1.3 Need for Research (motivation)	6
1.4 Objective of this Study	7
2 LITERATURE REVIEW.....	8
2.1 Composites.....	8
2.1.1 Metal Matrix Composites	10
2.2 Brief History of Friction Welding	13

2.3 Friction Stir Welding	15
2.4 Friction Stir Processing.....	19
2.5 Effective Parameters on Friction Stir Processing.....	20
2.5.1 Tool Geometry	21
2.5.2 Rotational Speed and Feed	25
2.5.3 Tilt Angle of Tool	26
2.5.4 Extra Parameters	26
2.6 Reinforcement Particles Size	29
2.7 Process Temperature.....	29
2.9 Effect of FSP on Mechanical Properties.....	35
2.10 Methods to Achieve Very Fine Grain Structure.....	36
3 METHODOLOGY	40
3.1 Materials	40
3.1.1 Properties of 7075T6 Aluminium.....	40
3.2 Ceramic Powder	42
3.3 Friction Stir Processing Tools.....	43
3.4 Equipment of the Friction Stir Processing.....	44
3.5 Fixed Parameters	45
3.5.1 Rotational Speed	45
3.5.2 Feed Rate	45
3.5.3 Tilt angle.....	45
3.5.4 Depth of tool penetration.....	45
3.6 Investigated Parameters	46
3.6.1 Number of Pass	46
3.6.2 Direction of tool rotation.....	46

3.7 Metallography	46
3.8 Tool Geometry	47
3.9 Hardness.....	47
3.10 Wear Properties	48
3.11 XRD Test	49
3.12 Tensile Test	49
4 RESULT AND DISCUSSION.....	51
4.1 Producing a Sample without Defect	51
4.2 Microstructure	51
4.3 Producing AL 7075/TiNNano-Composites	54
4.4 Effect of Number of Pass on Process	57
4.4.1Effect of Number of Passes and Tool Geometry, Direction of Rotation on Micro and Macro Structure of Samples	57
4.5 Effect of Tool Geometry in the FSP Process by Analyzing Mapping Pictures	63
4.6 XRD Analysis of FSP Samples	68
4.7 Mechanical Properties Tests	71
4.7.1 Wear Test (of FSP Samples)	71
4.7.2 Effect of FSP on Micro hardness	79
4.7.3 Effect of the FSP Process on the Tensile Properties of Material	82
5 CONCLUSION.....	84
6 REFERENCES	86

LIST OF TABLES

Table 1.1: Mechanical properties of aluminium.....	4
Table 2.1: Different parameters in tool design.....	22
Table 3.1: Chemical combination of aluminium alloy 7075.....	40
Table 3.2: AA 7075 properties.....	41
Table 4.1: Grain size values for different tool geometry and pass number.....	61
Table 4.2: Mass reduction of pin, disc, and mean friction coefficient for each sample.....	71
Table 4.3: The mechanical properties of FSP samples.....	83

LIST OF FIGURES

Figure 1.1: Percent of AL used in airplane manufacturing.....	4
Figure 2.1: Continues and discontinues phases in a complex material.....	9
Figure 2.2: Evolution chart of welding processes and history of their creation from start to till today.....	13
Figure 2.3: Shape of rotational friction welding	15
Figure 2.4: Friction stir welding tool.....	16
Figure 2.5: Views of friction stir welding.....	17
Figure 2.6: Examples of Different types of pins.....	23
Figure 2.7: Structures and possible defects resulting from different shapes of pin...24	
Figure 2.8: Effect of pin shape on 6061 hardness after FSP.....	25
Figure 2.9 General representation of tool tilt angle.....	26
Figure 2.10: Images of FSP surface in one pass and multi passes over aluminium..28	
Figure 2.11: Temperature distributions on different region of FSP in different state, zone III show the core of weld.....	30
Figure 2.12: shows the Effect of rotational speed to distance from weld center ratio on maximum temperature.....	32
Figure 2.13: Temperature on weld center in FSP of AZ31 magnesium alloy.....	32
Figure 2.14: Formed zone in friction stir processing.....	33
Figure 2.15: Thermo mechanical effected zone 7075 aluminium alloy.....	34
Figure 2.16: Submerged FSP.....	34
Figure 2.17: Fracture plane of AZ91 which indicate the onset of fatigue fracture crack via surface hole.....	35
Figure 2.18: Sever plastic deformation methods.....	38

Figure 3.1: Initial shape of work-piece.....	42
Figure 3.2: FSP Work-pieces with groove.....	42
Figure 3.3: FSP tools.....	43
Figure 3.4: Machine and fixture used in FSP.....	44
Figure 3.5: General figure of tool penetration.....	46
Figure 3.6: Etched, metallography sample.....	47
Figure 3.7: Optical microscop.....	47
Figure 3.8: Hardness tester.....	48
Figure 3.9: Mesurment equipmennt.....	48
Figure 3.10: Schematic picture of wear test machine.....	48
Figure 3.11: (A) show the disc picture (B) is picture of samples (C) show the region of FSP work-piece which wear samples cut.....	49
Figure 3.12: Tensile specimen and tensile machine.....	50
Figure 4.1: Surface of the samples after processing by no-pin tool (A) and tool with triangular pin (B).....	51
Figure 4.2: The microstructure of BM, TMAZ and SZ.....	52
Figure 4.3: Microstructure of (A) base metal (B) stir zone.....	52
Figure 4.4: (A) advancing TMAZ, (B) retreating TMAZ, (C) downward TMAZ...53	
Figure 4.5: Microstructure of FSP zone with good distribution of powder (A) and no good distribution (B).....	54
Figure 4.6: (A) SEM picture of SZ zone and (B) shows EDS analysis result of white point.....	55
Figure 4.7: OM picture of cumulative region in stir zone.....	55
Figure 4.8: (A) SEM picture of FSP sample (B) to (E) microstructure of showed regions in (A).....	57

Figure 4.9: Two passes samples (A), (C), (E) and 4 passes samples (B), (D), (F)...	59
Figure 4.10: Size difference between fine grains and large grains in different tools.....	60
Figure 4.11: Shows OM pictures of SZ; (A)(C)(E) show the two pass generated samples and (B)(D)(F) show the four pass generated samples, also (A)(B) and (C)(D) and (E)(F) show the threaded taper, triangular, and square tool samples respectively.....	62
Figure 4.12: SEM picture of stir zone.....	63
Figure 4.13: Shows the mapping of nano-powder in advancing side of samples generated by four pass parameters. (A),(D),(G),(J) pictures belong to the threaded taper tool,(B),(E),(H) and (K) are for square tool and(C),(F),(I)and (L) represent triangular tool pictures.....	65
Figure 4.14: Shows the nano-powder distribution in the retreating side of four pass samples ,for the square tool (A),(C),(G),(E) and for the triangular tool (B),(D),(F),(H).....	67
Figure 4.15: The XRD result of samples.....	69
Figure 4.16: Friction coefficient change in distance graphs for all samples.....	73
Figure 4.17: Macro pictures of pins and disc wear surface.....	76
Figure 4.18: The EDS analysis of pin surface.....	77
Figure 4.19: The EDS analysis of disc wear surface.....	78
Figure 4.20: SEM picture of wear surface.....	79
Figure 4.21: Hardness distribution VS distance from weld center.....	81
Figure 4.22: The average hardness of samples.....	82
Figure 4.23: Tensile samples after fracture.....	82

LIST OF SYMBOLS

AA	Aluminium Alloy
FSP	Friction Stir Processing
SZ	Stir Zone
HAZ	Heat Effected Zone
TMAZ	Thermo Mechanical Effected Zone
TiN	Titanium Nitride
TT	Threaded Taper Tool
T	Triangular Tool
S	Square Tool
HV	Hardness Vickers
MGS	Mean Grain Size
Gpa	Giga Pascal
Mpa	Mega pascal
Cu	Copper
Cr	Chrome
Fe	Iron
ZN	Zinc
OM	Optical Microscope
SEM	Scanning Electron Microscope

XRD	X-Ray Diffraction
EDS	Energy Dispersive Spectroscopy

Chapter 1

INTRODUCTION

1.1 Aluminium

Aluminium is a soft and light metal with silver gray appearance and thin oxide layer which is generated because of being in contact with air, and this prevents corrosion. The weight of aluminium is about one third that of copper, it is malleable and flexible. After iron, aluminium is the most used metal and is important in almost all sectors of industry[1]. Aluminium alloys are divided in two major groups, cast aluminium and wrought aluminium, in this research wrought aluminium is used.

1.1.1 Types of Wrought Aluminium

1.1.1.1 1xxx Alloy Series

It is aluminium with 99% or higher purity, this group of aluminiums is famous for high resistance to corrosion and high heat and electrical conductivity. Workhardening may cause slight increase in resistance for these alloys. The main impurity elements in these alloys are iron and silicon. These alloys are mostly used in electrical and chemical equipment, electrical and architectural transducers.

1.1.1.2 2xxx Alloy Series

Copper is the main impurity in these alloys. The alloys need heat treatment to achieve desired properties. When they are heat treated, the mechanical properties of these aluminiums are similar to low carbon steels. 2xxx series alloys under certain conditions may be subjected to intergranular corrosion. This group of alloys is used

for applications that require high resistance to applied loads like aircraft wings. These alloys cannot be welded and can be machined very well.

1.1.1.3xxx Alloy Series

The major impurity element of 3xxx series alloys is manganese. These alloys are not generally heat treatable. These Three 3003, 3004 and 3150 alloys are widely used in sectors requiring moderate resistance. Their applications include beverage cans, kitchen sets and road signs.

1.1.1.4 4xxx Alloy Series

The main impurity in these alloys is silicon. The maximum solubility of silicon in solid solution is at 577°C . These alloys have good forging capability and have a low coefficient of thermal expansion and are used in producing forged pistons of cars

1.1.1.5 5xxx Alloy Series

With 5 percentage of magnesium, most of these series alloys are not heat treatable. They are wrought alloys and have good weld-ability, corrosion resistance and have moderate strength when compared to other aluminium alloys. 5050 alloy with 1.2 % magnesium is used in automobile fuel pipes production and 5083 with a higher percentage of magnesium is used in marine structures.

1.1.1.66xxx Alloy Series

These series of alloys include sufficient amounts of silicon and magnesium which generates magnesium silicide, which is heat treatable. Although this series of alloys are not as rough as 2xxx and 7xxx series, they have good formability, weld-ability, and corrosion resistance and are used in architecture, transportation equipment, fencing and stair

1.1.1.7 7xxx Alloy Series

The major impurity element in these alloys is zinc, but also includes some magnesium, copper, and small quantities of manganese and chromium. This series of alloys have the highest tensile strength. Due to the existence of chromium, their tendency to corrode is minimized. They are also un-weldable alloys. Due to their high strength and high corrosion resistance these alloys are used widely in airplane structures, military equipment and missiles.

The use of aluminium has increased because of increasing energy prices. Its low weight, good mechanical properties and price has made more producers to gradually change steel products to aluminium products.

Aluminium alloys because of their high strength and low weight have many applications; they are utilized for their high electrical and thermal conductivities, ease of fabrication, and ready availability. Commercial pure aluminium is a weak metal and its tensile strength reaches its maximum at 13000 psi but by adding some elements such as manganese, magnesium, silicon, and copper, aluminium alloys can be produced. Through heat treatment and cooling operations, its tensile strength can reach 100,000 psi. As a conductor of electricity, aluminium has 62% the conductivity of copper. Its heat conductivity is high among metals and can be used as a heat exchanger; also it can be casted by any method and can be rolled to any thickness. In table 1.1 some mechanical properties mentioned

Table 1.1 Mechanical properties of Aluminium

Properties	Cast	Wrought
Tensile strength	42000 psi	80000 psi
Yield strength	22000 psi	72000 psi

One of these alloys is the 7xxx series aluminium alloy which has a strength-to-weight ratio comparable to titanium and steel alloys and are used especially in aviation (in upper wing skin) and transportation industry, where strength is one of most important factor in design.

Figure 1.1 shows the percentage of the aluminium which is used in manufacturing an airplane

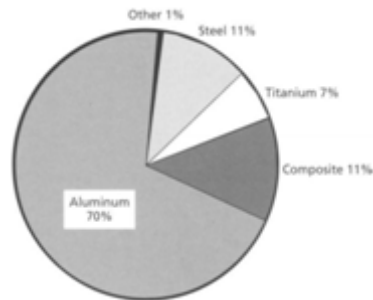


Figure 1.1 Percent of AL used in airplane manufacturing [40].

A new group of materials that show good strength, high hardness and corrosion and wear resistance, are metal matrix composites. Although obtaining a uniform distribution of ceramic particles on a matrix metal with traditional surfacing methods is difficult, metal matrix composites can be produced by different methods, like powder metallurgy, mechanical alloying, laser processing technique, and other casting methods. Between all these methods, casting methods or methods that produce composites from a melted face of the base metal are the most used, because of their

high speed and low cost, they have more attention in mass production of industrial parts compared of other methods. In recent years friction stir processing (FSP) has also been used in order to produce metal matrix composites.

Friction stir processing originates from the modification of the microstructure of metallic materials, which develop on the base during friction stir welding [2].

In this process a rotational tool with a specific design that includes a pin and shoulder penetrates into a metal sheet. Then the tool moves on the sheet in a determined direction. Due to the friction between the tool's shoulder and the surface of the sheet, heat is generated and makes the material soft in the processing zone. With the generated mechanical friction by tool's pin, materials in the processing zone undergo severe plastic deformation and a dynamical recrystallization is created on it. The result of the process is a homogeneous microstructure with fine coaxial grains under the processing region produced. Also using this process, producing a composite layer on the sheet surface is possible. To produce a composite layer, firstly a groove is machined on the part surface and ceramic powder in nano size is used to fill the groove. Then friction stir processing can be started on the work-piece. Because of the mechanical friction of tool pin, the ceramic powder is distributed in base metal. The consequence of this process is a composite layer with fine grain size and uniform distribution of ceramic powder on the surface of the part.

1.2 Definition of the Problem

Producing aluminium base nano-composite by friction stir processing

1.3 Need for Research (motivation)

FSP is relatively novel method which was recently used as a technique to generating surface composites and modification of mechanical properties. This process possesses superior trait compared to conventional composite generating methods due to its cost efficiency, flexibility and less defects during processing. FSP has achieved high consideration in recent years, but as it is still a novel method and its effective parameters are under development, commercially application of this method is not widely expanded. One of these important parameters is tool geometry which has a very significant effect on the properties of the FSP zone such as grain size and nano-powder distribution. Additionally, the effect of this factor can be differed by changing the material and nano-powder that used.

On the other hand it has been predicted that there will be a major increase in traveling by aircraft in the next decades. Due to this high demand, long hours and distance of these flights, also new generation of aircrafts which require higher performance, and demand for materials with higher capability especially in the military sector, there is the need to revise usage of traditional material in these sectors, one of the methods that can be considered as a solution is the usage of FSP process to make new composites, with better properties and low cost than traditional materials which are currently used. Aluminium 7075 is one of the most used alloys of the aluminium alloys series, especially in aerospace and military fields, that is why increasing the mechanical properties by finding the microstructure and generating new composition of this alloy seems very significant to new developments in aviation and military sectors.

1.4 Objective of this Study

1. The main aim of this research is producing non-composite between TiN and 7075 aluminium by applying friction stir processing on 7075 aluminium to increase the wear properties by using different tool geometry.
2. The effect of tool geometry will be examined on the experimental material
3. Investigating mechanical properties (hardness, tensile, wear) of the zone under process.
4. The effect of adding nano-powder on experimental material
5. Investigating the nano-powder distribution in FSP zone
6. Investigating the microstructure of FSP zone
7. Studying the effect of changing tool rotation direction on nano-powder distribution
8. Studying the effect of the number of passes on mechanical properties
9. Investigating the FSP zone for new intermetallic phases.

Chapter 2

LITERATURE REVIEW

2.1 Composites

Nowadays the world is witnessing a growing need to use a blend of materials to achieve desired properties because generally it is difficult for a single material, to meet all required properties, according to economical and performance aspects. Composite materials are built by the combination of two or several materials to achieve unique mixtures of properties. These materials keep their physical and chemical properties and create apparent boundary with each other. The mixture as a whole depending on some criteria develops better properties compared to each of its basic components.

In composites, generally, there are three separate zones, including (1) continuous phase (Matrix), (2) discontinuous phase (reinforcement) and (3) the boundary layer of this two phases determines the properties and characteristics of the composite.

Continuous phase (matrix) is divided into three groups:

- (1) Metal: metal matrix composites
- (2) Polymer: polymer matrix composites
- (3) Ceramic: ceramic matrix composites

Discontinuous phase is often divided in three general categories

- (1) Powder particles

(2) Planar particles

(3) Fibers (long and short) each sort creates specific characteristics in the composite.

Figure 2.1 shows different phases in the composites.

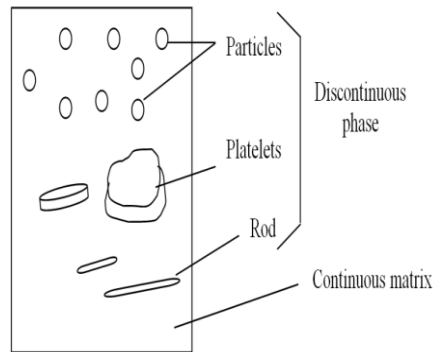


Figure2.1 Continues and discontinues phases in a complex material

In particle composites, properties do not depend on direction, whereas in fibercomposites the direction is very important. In a composite, generally fibers admit load on the structure. Whereas in matrix phase, fibers keep a favorable location and form a load transfer medium between leafs, as well as keep fibers protected from environmental damages caused by increasing temperature and humidity and etc. Most of the composite materials, reinforced by fibers, perform a combination of strength and module that is similar and even better than metal materials. Due to the low density of the material, strength to weight ratio (specific strength) and module to weight ratio (specific module) are significantly superior to metallic materials. Therefore composites reinforced with fibers form a major group of engineering materials that can be used in many applications wherelight weight is important, such as automobile industry, aerospace, etc, instead of metals.

Composites reinforced with particles such as steel and aluminium, are usually considered to have isotropic structure, because they demonstrate almost same

properties in all directions. Properties of fiber reinforced composites generally are much reliant on measurement direction.

For instance tensile strength and module for a reinforced layer in a one directional fiber in the length direction is Maximum. However, if the properties are measured at other angles, the values obtained will be lesser than in the length direction. For other mechanical and physical properties such as coefficient of thermal expansion, coefficient of thermal conductivity, etc there is still such angle dependency.

Therefore designing a structure reinforced with fibers is difficult than a structure reinforced with particles and that is mainly due to difference of properties in different directions of composite fibers. Despite this fact, the non homogenous nature of reinforced fiber composite materials can be applied to consciously strengthen a structure in major stress direction, raise hardness in particular direction, manufacturing structure with zero thermal expansion and etc [3].

2.1.1 Metal Matrix Composites

Metals are suitable materials for engineering materials; they have a wide range of controllable properties. These properties can be controlled by alloy elements and thermo mechanical processes. Extensive use of metals is not only related to high hardness and stiffness but also low price and ease in engineering parts produced with a wide range of production methods. To achieve desired properties, metal matrix must be combined with proper strengthener.

Certainly the cost of achieving such improved properties is one of the challenges in applications that present potential in the use of metal matrix composites.

There are many reasons why designers and engineers tend to use metal matrix composites parts apart from increase strength and stiffness requirements.

Composites are capable of providing selective properties for many specialized applications; they can also acquire a range of mechanical and physical properties from ceramic and metals sets. Some important factors to be considered are: improvement of strength in high temperature, module improvement, creep resistance, weight reduction, increase ratio of strength to weight and reduction in the coefficient of thermal expansion. In metal matrix composites a wide range of metals and alloys such as aluminium alloys, copper alloys, cast iron, steel, magnesium alloys and nickel base super alloys, titanium alloys, zinc alloys and etc are used.

Generally, a metal matrix composite system can be produced very easily using a matrix from one metal alloy that is strengthened with ceramic as reinforcement. For instance AL6061/30v/SiC has been made by an aluminium alloy reinforced with 30 % volume of silicon carbide. Metal matrix composites are softer and stiffer compared to ceramic matrix composites (CMC). The goal of reinforcing the metal matrix composites is to increase the strength and module, they look like polymer matrix composites but in ceramic matrix composites, reinforcement decreases damages made by distortion.

In order to select the matrix alloy for the metal matrix composite several considerations have to be made. Attention should be placed on the profile of reinforcement (powder particles, long or short fibers) because the shape of the particles in the matrix has a significant influence on the properties of the resultant

matrix. Using long fibers as reinforcement, may cause, transmission of a large amount of applied load to the reinforcement.

The strength of this kind of composites increases with an increase in the strength of the fibers used in it. The main function of matrix alloys is to better transfer load to fibers and prevent them from crack growth when fiber failure occurs. Hence, alloy matrices in metal matrix composites that are reinforced with long fibers (continues), are mostly selected from tough materials than a high strength material. For metal matrix composites reinforced with short fibers (discontinues) it is possible that matrix has effect on the strength of the composite. As a result increasing composites strength leads to strengthen alloy matrix.

Comparing with other type of composites (polymer matrix and ceramic matrix), metal matrix composites contain special combination and varying production processes. This problem is mostly due to inherent differences between metal, ceramic and polymer. Metal matrix composites are made by different methods such as powder metallurgy; make diffusion bounds, casting methods and mechanical alloys. Among these methods, casting methods or methods that produce composites from molten phase metal at high speed and low price compared to other mass industrial parts production.

Also some welding methods such TIG and leaser welding are used to make plane composite layer[3].

2.2 Brief History of Friction Welding

In today's modern world there are many different methods used to construct welding between different metals. These methods are categorized by considering different aspects, from common oxyacetylene torch techniques to laser welding methods.

One of conventional techniques in the classification of these methods is fusion welding and solid welding. In fusion methods, chemical combination of metals in molten state arises and may be done with the use filler materials or consumable electrodes. Also the process may need a neutral environment to prevent oxidation. This environment can be achieved with the use of molten materials or protective gases. Sometimes it is necessary to prepare the surface of the part before welding.

Figure 2.2 show different welding methods in order of their invention.

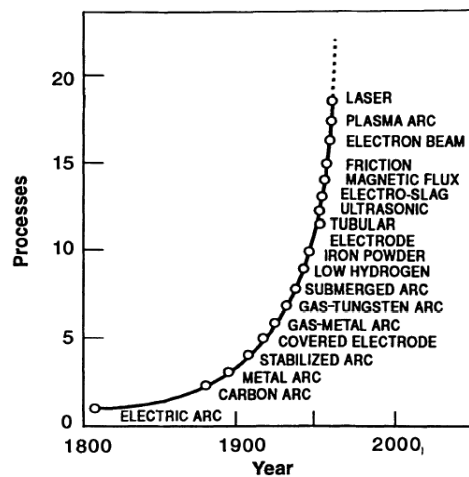


Figure 2.2 Evolution chart of welding processes and history of their creation from start to till today [4].

Conventional methods such as TIG, MIG and laser welding are part of fusion processes. Many problems and defects in such methods occur due to melting and freezing. Melting and freezing cause loss of mechanical properties such tensile strength, fatigue and ductility. Other disadvantages of these methods are porosity,

oxidation, heat and cold crack, and limitation in welding of dissimilar materials with different thermal conductivity coefficients. Solid welding is a process in which welding occurs at a temperature lower than base metal melt point.

As a result oxidation does not occur and there is no need to use protective gas, neutral environment, and consumable material. Methods such as, friction welding, explosive welding, ultrasonic welding, forging welding are solid state processes. Each of the three important parameters: time, temperature, and pressure with help of other parameters or together create a weld joint.

According to this fact there is no need to melt material in this method, as a result there are fewer defects in these method compared to fusion techniques. In this method, the heat affected zone which is a common reason for most of the reduction of mechanical properties is very small. Dissimilar materials easily weld each other and the coefficient of thermal conductivity is lower than other fusion methods [4].

In friction welding, the process occurs without any electrode filler, heat generator, or neutral environment. Friction welding generally is divided in 3 groups:

- (1) Non-rotational friction
- (2) Rotational friction and
- (3) Stir friction

Friction welding process use mechanical energy to generate heat and plastically deform the part. Rotational friction welding is the first commercially used friction welding process. In this method one of cylindrical parts rotates in one direction while

the other is fixed rotational part. Materials are softened in the cross section, and subsequently forged to each other; Figure 2.3.

This process is used for similar and dissimilar metals. This process is finished with, temperature generated from the fast motion and the pressure on both parts, as they move past each other and plastic material is extruded from the contact region of two parts to the outside. To achieve a good welding junction with desired strength, after stopping the rotation, and before cooling, the two parts are compressed on each other with more force.

The result of this process will be welded junction formed in solid state and will not have fusion welding problems.

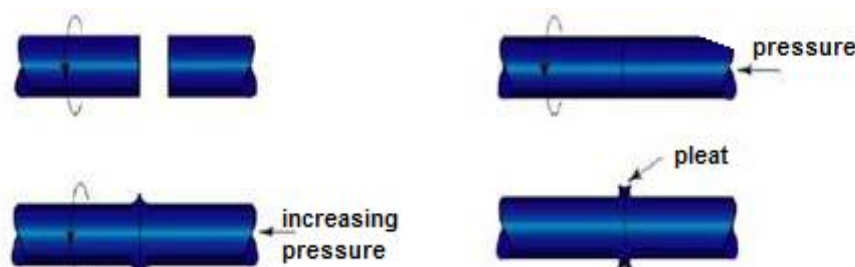


Figure 2.3 Shape of rotational friction welding [4].

In non rotational friction welding, alternating liner orbital and angular motions are used to weld square and rectangular belts [4].

2.3 Friction Stir Welding

Friction stir welding carried out in 1991 at England welding institute and for first time experimented on aluminium. In this process the first aim is a made junction between the materials whose welding with fusion methods is difficult [5, 6, 7, and 8]. The Friction stir process is developed from a process of friction welding. In

conventional friction welding, the heat generated due to friction in the edge of the two faces, rubbing with each other, but in this process the third piece is in the shape of a non consumable (resistance to abrasive) small rotational tool rubbed at the two joining surfaces. The tool in this process consists of two important parts which include shoulder and pin. Each of these two parts may have different designs, which can be verified depending on their profiles, the process parameters and result specifications. Figure 2.4 shows a friction stir welding tool.

The tool's shoulder which is in contact with the surface of the work piece due to friction provides essential heat for making softer the material in the process zone. The tool's pin put the material under sever stirring and plastic deformation. The process begins with clamping the metal sheet on a plane called backplane then, the sheet must be settled correctly with a clamping force to preventing movement in different directions during processing.

Then rotational tool penetrates in to the interface of components so that the shoulder touches the part surface, in figure 2.5. The tool has two main motions:

- (1) Rotational motion to generate friction and heat and turbulence
- (2) Feeding motion to continue the welding operation.

In addition, the tool during rotation is compressed on the junction spot. Contact pressure causes more frictional heat and forged materials in junction region.

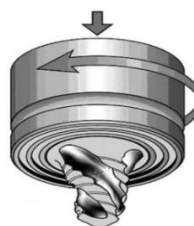


Figure 2.4 Friction stir welding tool [5].

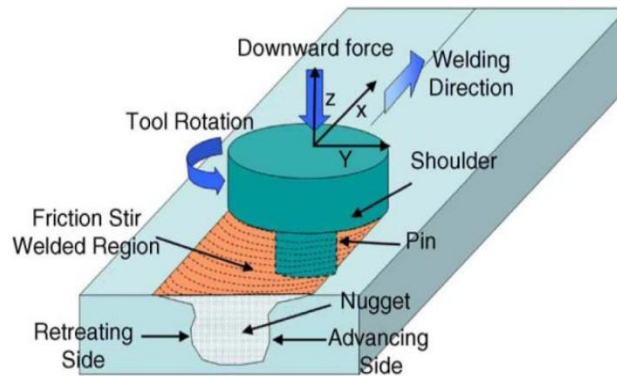


Figure 2.5 Views of friction stir welding [5].

Heat is generated due to (1) friction between tool and work piece (2) plastic deformation of material. Localize heating makes the material soft around the pin and combination of feed and rotation of the tool causes transmission of material from the advanced side of the pin to its back. Because of the complex geometrical shapes of the tool, the model of material flow around the pin is very complex [5]. The crystal structures of this process due to severe plastic deformation at high temperature are fineequiaxed recrystallized grains; which improve mechanical properties [6, 9].

In this process since the material does not melt and welding is made indoughform, there is no sign of defects formed during casting and solidification, but instead other defects such as tiny tunnel holes and cracks formed in final structure [9]. However these defects are very easily eliminated and controlled by adjusting the process parameters.

The advantages of this process are reducedenergy consumption and minimal part distortion. There is no need for protective gas, no environmental damage, no need to filler materials, no production of toxic gases and vapors, good tensile strength and fatigue of produced parts.

Friction stir welding is not limited to any specific condition or position and it can be used in any condition, because there is not any melt pool in this welding. It is a very simple process and unlike fusion welding does not require skilled operator, so an operator with less experience can make welds with no defect. It is possible to welding complex parts with this method. This is a clean method and does not produce gas, harmful radiation, and toxic fumes and does not require high safety. This welding is not perceptible on the surface and it is not necessary to clean oxide layer and same operations which done in fusion welding [4].

Aluminium alloys rapidly form, surface oxide. As a result welding these alloys must be done in a short period after cleaning the oxide layer, to avoid re-oxidation. This problem is one of the major troubles in aluminium alloys welding.

This method is appropriate for welding aluminium alloys especially 2000, 6000, 7000 series which belong to non-weldable aluminium series and are welded via fusion methods, which cause defects such as heat crack and porosity. Heat treatable 7000 and 2000 alloys are scarcely welded due to cracks and porosity formed during fusion welding methods and gases like hydrogen easily solute in the welding pool.

Other problems arise when these alloys are affected by heat which is generated due to welding and this heat causes phase changes and mechanical properties decrease. Hence welding this two series of alloys to each other is one of the major applications for friction stir welding [4].

Khodir et al [10] by welding 7075 and 2024 aluminium alloys investigated the effect of welding speed and placement of sheets in advance or retreat side, on microstructure and mechanical properties. Also Kavalieri et al [11] did some research on mechanical properties and weld microstructure of 7075 and 2024. They choose 700 rpm rotational speed and 2.67 mm/s feed rate. 7075 alloy is placed in advancing side and 2024 in retreating side. Finally they welded the two parts successfully and there was no sign of surface defects and porosity, after tensile test result showed that the ultimate strength of 7075 alloy junction is extremely high, and strength in 7075 to 2024 and 2024 junction is same. But stiffness and elongation of 2024 junction is higher than the rest.

One of the aspects that convinced manufactures to use this method is long life of tool in most of metals, and no need for electrode and filler, for instance with an ordinary welding tool, welding of 1000 meter of 6000 series alloy is possible simply [4].

2.4 Friction Stir Processing

Friction stir processing recently innovated by Mishra et al [12, 13] is a process used to improve microstructure of metals; which is based on friction stir welding primary principles. Fundamentals and parameters of these two methods are same but there are some minor differences, there is no difference in microstructure changes and material properties.

The aim of FSP is not to join two parts, but rather to improve structure, change grain size, increase strength, uniform structure of grain size, sediments distribution and make surface composites. In friction stir processing the tool's pin penetrates into an

integrated part, in order to obtain desired properties in the metal, and make localized microstructure changes.

For instance using friction stir processing on 7075 aluminium alloy makes use of the high strain rate super plasticity property [14, 13]. Also this process is used to produce surface composites, homogenization of parts produced by powder metallurgy, refine microstructure in metal matrix composites improve properties of casting alloys [16, 15]. Same as in friction stir welding, for the first time friction stir processing was done on aluminium. Mishra et al [15] produced an Al/SiC composite layer by this method and showed that reinforced SiC particles were distributed well in aluminium matrix. Hsu et al [17] increased the young's modules and tensile strength of aluminium with production of Al/Al₃Ti nano-composite.

They showed that the young's modules of the produced composite layer, increased with increase Al₃Ti percent. By adding 15% titanium, young's modules increased to 114 GPa which is 63% more than aluminium's young's modules. Shafiei et al [18] produced Al/Al₂O₃ nano-composite by using friction stir processing with a different number of passes and investigated the microstructure and the wear properties of the composite layer.

2.5 Effective Parameters on Friction Stir Processing

Friction stir processing involves plastic deformation and severe flow of material. Parameters of Welding and tool geometry determine the flow pattern and temperature distribution; As a result has direct effect on final microstructure of the region under process [5,6]. In this part effective parameters on friction stir processing are explained briefly.

2.5.1 Tool Geometry

Friction stir processing tool geometry determines the material flow and speed of material flow and plays an important role in this process. The difference between pin shapes causes differences in the contact face with the material and affects material relocation; heat generated, and required force for welding and etc [5, 19, 6, 9].

The tool in friction stir processing has two main functions

- 1) Generate localized heat in order to change the material to plastic form
- 2) Adjust the plastic flow of material

In the first step and when the tool moves down, primarily heat is generated via friction between pin and part. The excess generated heat is due to material plastic deformation.

The tool moves lower so that shoulder touches the work piece. Friction between the shoulder and the work piece causes extra heat. The rate of heat generation is most dependent on the ratio of shoulder diameter to pin diameter than other parameters. The second function of the tool is agitation, turbulence, and flow in material. Since uniform microstructures and properties are due to good tool design, the required force for welding is also reduced by appropriate tool design. Generally concave shoulder and threaded cylindrical pins shapes are used. By increasing skill and understanding of the material flow, tools have been developed with different geometries [4].

Tool geometry can be affected by factors such as torque, amount of forces generated and heat generation rate. The main geometry factors are the length, diameter of pin and shoulder diameter. The length of the pin depends on the thickness of the layer,

from the surface of the work piece which will be refined. Shoulder diameter usually is considered 2 to 4 times bigger than the diameter of the pin [5].

Other parameters that also can be considered in tool geometry design are mentioned in table 2.1. These particular geometries are applied on the pin.

Results of these changes are given in the last column of the table. It should be noted that good or bad results cannot give a certain answer and the aim is to obtain quality in the layer of the product surface. In the end the optimal geometry for the tool, is obtained after several different tests and research on the generated surface layer.

Table 2.1 Different parameters in tool design

Row	Parameter	Variable	Effect on process
1	Diameter of the pin	Increase or decrease in pins diameter	Perpendicular force – generated torque
2	Making grooves on pin, in the pin direction	Number and deeps of grooves	Increasing or decreasing material flow –change in generated temperature
3	Using taper pins	Taper angle	Perpendicular force – generated torque
4	making Threaded on pins	Pitch of thread	Increasing or decreasing material flow –change in generated temperature

The tool's Pin has different shapes. Ellangovan et al [21, 9] carried out research on the effect of different pin shapes. The tested shapes were: straight cylindrical,

threaded, cylindrical, taper, triangular and square. Figure 2.6 presents a picture of these tools.

The results showed that square pin gives sound structure and better mechanical properties.

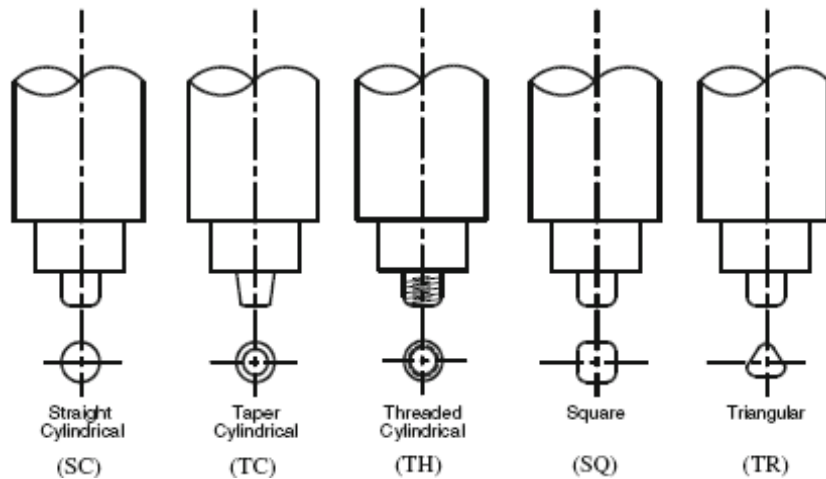


Figure 2.6 Examples of Different types of pins [9]

Square and triangular pins cause a disturbance pulse in the material. For example, when the tool is rotating at a speed of 1200 rpm, the square pin generates 80 pulses per second and the triangular pin 60 pulses per second. Cylindrical, taper and threaded pins do not generate pulse. With higher number of pulses, the size of the final grain will decrease. Also the substance distributes uniformly and as a result strength and hardness will be higher [21, 9]. Elangovan et al experimental results are shown briefly in figure 2.7.

Cylindrical pin













Axial Force (kN)	Macrostructure		Size of FSP zone (mm)		Shape of FSP zone	Name of the defect and location	Quality of weld metal consolidation	Probable reason
	RS	AS	W	H				
6			10	5.9	Elliptical	Tunnel defect at the retreating side and zig zag line at the advancing side	Poor	In sufficient axial force and inadequate heat generation
			8.0					
			5.6					
7			11.3	5.9	Inverted trapezoidal	No defect	Good	Sufficient heat generation and flow of plasticized metal
			6.2					
			4.7					
8			11.2	5.9	Elliptical	No defect	Good	Additional axial force leads to excess heat input and thinning of the weld zone
			5.8					
			4.9					

Figure 2.7 Structures and possible defects resulting from different shapes of pin [9].




Taper pin

Axial Force (kN)	Macrostructure		Size of FSP zone (mm)		Shape of FSP zone	Name of the defect and location	Quality of weld metal consolidation	Probable reason
	RS	AS	W	H				
6			7.9	5.9	Straight	Tunnel in top and bottom of the weld at retreating side	Poor	Insufficient heat input and inadequate metal flow
			5.2					
			4.3					
7			8.6	5.9	Inverted Trapezoidal	No defect	Good	Flow of the plasticized metal is adequate due to sufficient heat generation
			6.2					
			4.1					
8			9.7	5.9	Stretched Trapezoidal	No defect	Good	Additional axial force leads to excess heat input and thinning of the weld zone
			6.7					
			5.6					

Threaded pin

Axial Force (kN)	Macrostructure		Size of FSP zone (mm)		Shape of FSP zone	Name of the defect and location	Quality of weld metal consolidation	Probable reason
	RS	AS	W	H				
6			10.9	5.9	Elliptical	No defect	Good	Threads on the pin produces additional heat
			6.4					
			4.4					
7			11.2	5.9	Elliptical	No defect	Good	Extra downward movement to the plasticized metal that accelerate material flow
			6.7					
			4.6					
8			11.4	5.9	Elliptical with shear lips	No defect	Good	Excess heat input due to additional axial force reduces thickness of the plate in the weld zone
			6.3					
			6.2					

Square pin

Axial Force (kN)	Macrostructure		Size of FSP zone (mm)		Shape of FSP zone	Name of the defect and location	Quality of weld metal consolidation	Probable reason
	RS	AS	W	H				
6			11.3	5.7	Inverted Trapezoidal	No defect	Good	Sufficient flow of the metal by pulsing action of the pin profile
			6.7					
			4.1					
7			12.1	5.6	-do-	-do-	-do-	Eccentricity of the pin profile causes dynamic orbit with associated pulsating action resulted in good weld.
			6.7					
			4.6					
8			11.8	5.9	Inverted Trapezoidal with shear lips	-do-	-do-	Excess heat input due to additional axial force reduces thickness of the plate in the weld zone
			7.1					
			5.3					

Triangular pin




Axial Force (kN)	Macrostructure		Size of FSP zone (mm)		Shape of FSP zone	Name of the defect and location	Quality of weld metal consolidation	Probable reason
	RS	AS	W	H				
6			11.2	5.7	Inverted Trapezoidal	No defect	Good	Sufficient flow of the metal by pulsing action of the pin profile
			6.3					
			5.1					
7			11.4	5.8	Inverted Trapezoidal	No defect	Good	Sufficient heat generation with adequate flow of metal
			6.1					
			4.3					
8			11.8	5.9	Inverted Trapezoidal with shear lips	No defect	Good	Additional axial force increases the heat input and reduces the thickness of the plate in the weld zone
			7.1					
			6.8					

Figure 2.7 Structures and possible defects resulting from different shapes of pin [9].

The shape of the pin also affects hardness. Figure 2.8 show the result of Elangovan experiments on 6061 aluminium alloy

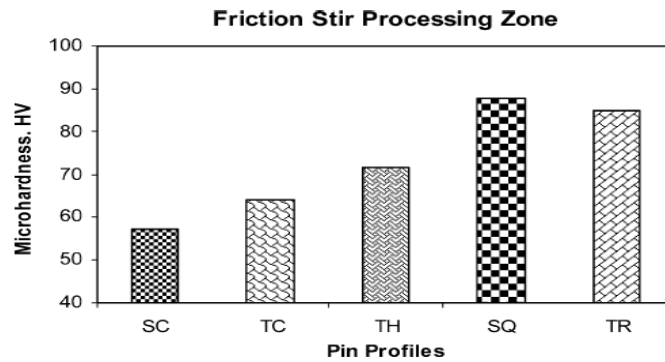


Figure 2.8 Effect of pin shape on 6061 hardness after FSP [9].

In this figure, SC indicates cylindrical pin, TC taper pin, TH threaded pin, SQ square pin and TR triangular pin [6].

2.5.2 Rotational Speed and Feed rate

In friction stir processing there are two important parameters: (1) rotational speed of the tool in the clockwise and anticlockwise directions and (2) feed rate of tool on work piece. Tool rotation on surface causes friction and mixing of material around the pin and also pin feed causes material transfer from the advance to the back part of the pin [22].

By increasing rotational speed of tool, the generated heat and mixed material increases. But it should be considered that with increasing rotational speed of tool the friction coefficient of the surface will change [5, 22]. By increasing rotational speed of tool the generated heat will increase due to friction and plastic deformation. By increasing heat, grain growth during recrystallization elevate and as a result grain size increase. However increasing feed rate causes reduction in the grain size. Because by increasing the feed rate, the duration which the material is under process and its generated heat reduces. This causes slower grain growth during recrystallization and grain size reduction [23].

Therefore, in order to achieve fine structures, rotational speed should be less and the feed rate be higher, but of course it should be considered that by applying this parameters, less heat is generated and this may require heating to make the material soft and less plastic deformation can be obtained[22, 23, 19].

2.5.3 Tilt Angle of Tool

It is one of effective parameters on welding quality. Previous experiences showed that, the value of this angle can be changed between zero to 5 for different materials, also for most materials the best value is 2 to 3.5 degree [5]. Figure 2.9 shows the general representation of friction stir processing with tilt angle clear on it.

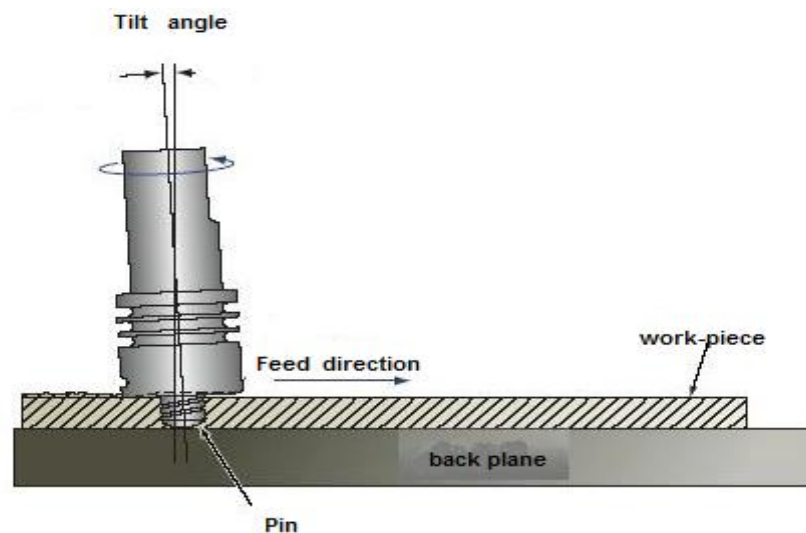


Figure 2.9 General representation of tool tilt angle.

The tilt angle of the tool causes the trapped material during tool penetration and feed under concave area of the tool to change to plastic form, and this material by using the force generated at the rear of tool reverses into the work piece with great pressure, this process is one of reasons for high strength and uniform structure in welding.

2.5.4 Extra Parameters

Pin penetration rate into the work piece, also affects the result of fine structure and properties. When the depth of penetration is undersized, the shoulder does not touch

the surface and cannot force the materials from advance side of the pin to the retrieve side of it, and the tunnel holes generated in final surface.

Lim et al [25] researched on the effect of depth of penetration, on distribution of carbon nano-tubes in the stir zone. They came to an understanding that with increasing depth of penetration, no defect occurred in the cross section of the samples and the nano-tubes distribution improved.

In some materials with high melting point such as steel and titanium and high thermal conductivity like copper the generated heat via friction may not be enough to soften and plastically deform them. In this cases work piece preheated, or an external heat generator is used during welding to increase the ratio of shoulder diameter to pin diameter. In materials with low melting point also, material must be cooled to prevent overgrowth of grains [19, 26].

Another important parameter is the number of process pass; process may be done in one pass or sometimes to achieve desired properties done in multi passes. Pass can be done completely or in certain size overlap each other. Figure 2.10 shows a picture of one pass and multi pass process on aluminium [8]

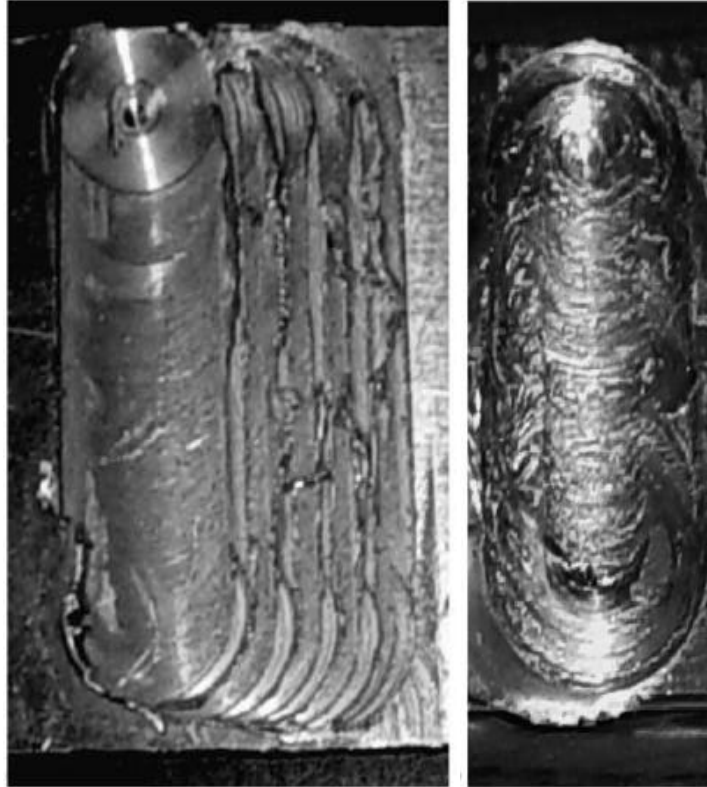


Figure 2.10 Images of FSP surface in one pass and multi passes over aluminium [8].

Shafiei et al [18] investigated the effect of pass number on powder distribution, hardness and wear properties of aluminium after friction stir processing with and without the presence of alumina (Al_2O_3) powder. According to their report increasing the FSP passes in samples with powder, powder distribution in aluminium matrix improved. Hardness of samples produced with four passes, is three times greater than the base metal and its wear rate is also less than the base metal.

They also reported that in samples without using powder, by increasing the number of passes, hardness decreased and finally in four pass samples it is less than base metal. Sato et al [27] showed that multi pass FSP in AZ91 magnesium alloy generated uniform micro structure with 2.7 μm grain size.

The main failure strain of the sheet with FSP applied on it with the mentioned microstructure in the FLD diagram is 6 times more than initial die-cast sheet.

2.6 Reinforcement Particles Size

Generally in metal matrix composites, reinforced with particles, the reinforcement particle size and the volume of the particles are the major factors affecting the microstructure and as a result on mechanical properties of the generated composites. By assuming the reinforced particles, distributed separately in metal matrix, the Zenz parameter can be used to calculate the theoretical grain size of composite layer. Size of the grain (dz) can be calculated by using equation 2.1 [28].

$$dz = \frac{4r}{3V_f} \quad (2.1)$$

In this equation (r) is the radius of the reinforced particle and V_f is the fraction volume of the reinforced particles to matrix phase. According to the equation by decreasing the size of the reinforced particles or increasing volume fraction, the size of grains in the composite layer is reduced.

2.7 Process Temperature

The fundamentals of FSP process are based on thermodynamic changes and the temperature of the process play an important role in the microstructure and final properties. In addition, temperature distribution in work piece is important [23, 29].

Process temperature, depends on rotation speed and feed rate variation. But generally, these parameters are selected in a way that the temperature of the weld in the zone is 0.7 to 0.9 of the melting point of the metal. (For instance temperature of process zone of AZ31 magnesium alloy is 420 to 580⁰C, whereas the melting point of

this alloy is 618⁰C [29]. The following empirical equation shows the relation between temperature of weld nugget, rotational speed and feed rate parameters.

$$\frac{T}{T_m} = K \left(\frac{W^2}{v \cdot 10^4} \right)^\alpha \quad (2.2)$$

In this equation T_m is the melting point of the alloy, T is the temperature in nugget of weld, W rotational speed, α and K are constant values depending on the base material. For magnesium alloys with 610⁰ C meltingpoints, K and α values respectively are 0.0442 and 0.8052 [23].

The temperature of the process, cooling rate and the time which the temperature of the process zone stay higher than recrystallization zone affects the microstructure and the final grain size and as a result on mechanical properties. As the temperature and the process time becomes higher, grain growth and final grain size would be higher. By increasing cooling rate finer grain size can be achieved.

In terms of tool geometry, generated heat during process mostly depends on the shoulder diameter and by increasing it, generated heat increases. Increasing the applied pressure and ratio of rotational speed to tool feed rate, also has same effect [29, 23]. Figure 2.11 shows Comminet al [23] experimental result on AZ31 alloy.

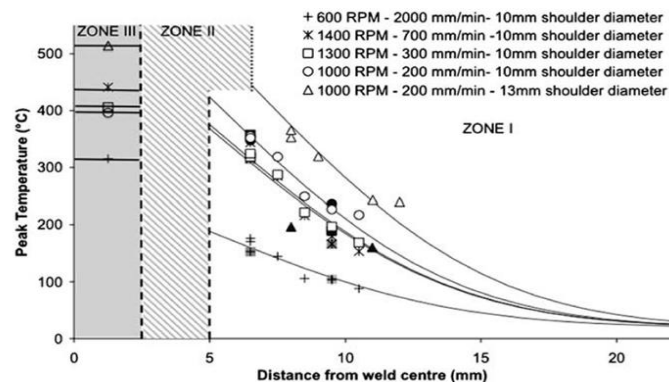


Figure 2.11 Temperature distributions on different region of FSP in different state zone III show the core of weld[23].

Determination the temperature distribution in stir zone (SZ) is difficult because of servo deformation on it; hence they mostly find the maximum temperature according to the formed microstructures after the welding process or with locating thermocouple near the pin and in proper places.

For instance the research done by Rhodes on welded 7075 aluminium microstructures showed that large sediment dissolve in the stir zone. Consequently, he find out the maximum temperature of process is 400 to 480⁰C. In addition Murr et al [30] find out that some of large sediment did not wiped out during welding and the resulting temperature rise of 400⁰C in 6061 aluminium.

Some other researchers used this method, in this field, finally can conclude these three points:

- (1)Maximum temperature is observed in SZ.
- (2)The temperature in SZ increases in the direction of the bottom ofthesurface of the sheet.
- (3)The maximum generated temperature is observed in the upper point of SZ.

Tang et al [31] also investigated the effect of rotational speed on the temperature of the field; the result showed that by increasing rotational speed, maximum temperature increased. Figure 2.12 shows the effect of rational speed, on maximum temperature at different distances from the center of the weld.

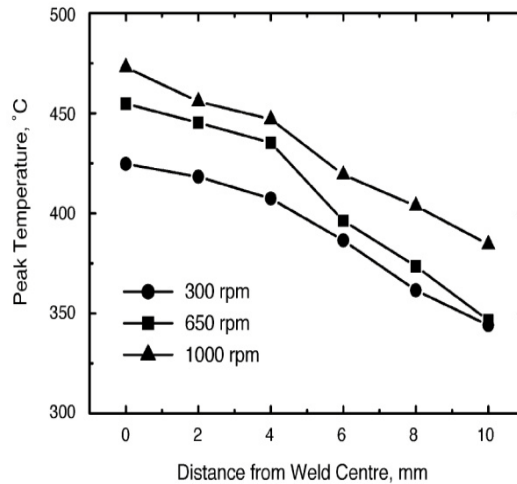


Figure 2.12 Shows the Effect of rotational speed to distance from weld centre on maximum temperature

Darras et al [6], research about the effect of rotational speed and feed on temperature history of the weld nugget in friction stir processing of AZ31 magnesium alloy. By increasing rotational speed or reducing feed rate, the maximum temperature increases and the time which the material is affected by high temperature increases.

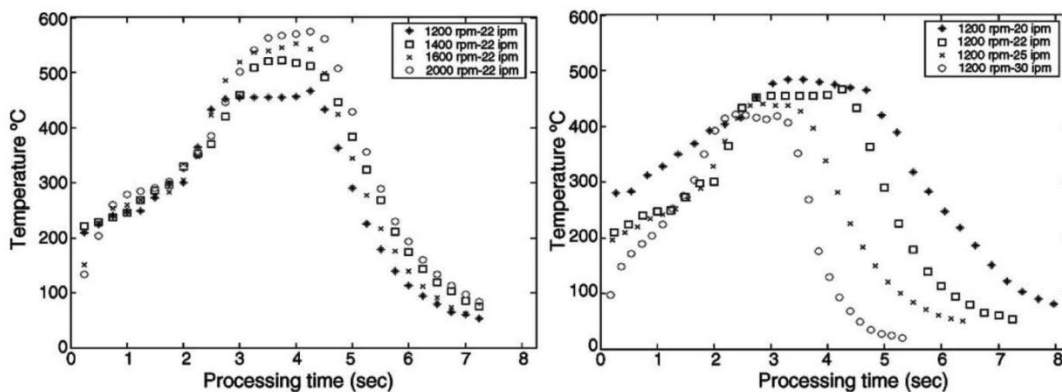


Figure 2.13 Temperature on weld center in FSP of AZ31 magnesium alloy

2.8 Microstructure changes

Severe plastic deformation and high temperature in stir zone during friction stir processing causes a form of recrystallized structure which solvates the deposits. [6, 19] By considering microstructure, grain size, size and shape of sediments, three zones

in FSP part are recognizable: nugget zone (NZ) or stir zone (SZ), thermo mechanical effected zone (TMEZ) and heat affected zone (HAZ), Figure 2.14.

The Microstructure of each zone, because of process parameters, changes severely and has great influence on the work piece mechanical properties [5]. In stir zone, severe plastic deformation and process generated heat, causes a recrystallized and fine grain microstructure. Grain size in this zone is influenced by generated heat via rotational speed and feed rate and tool geometry. The existence of sediment phases in this zone solvate.

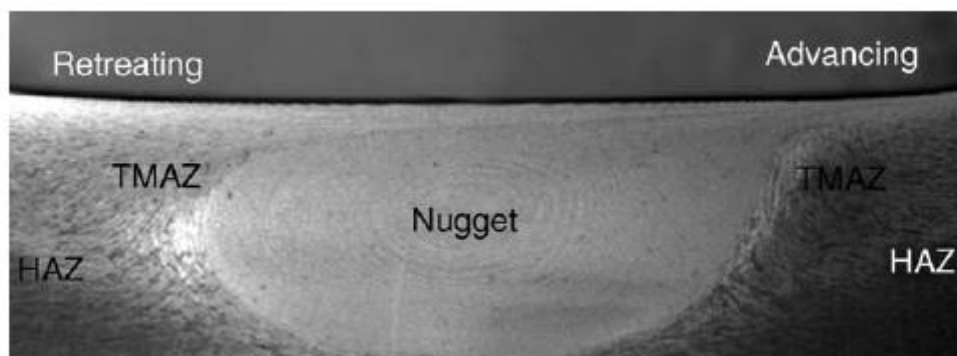


Figure 2.14 Formed zone in friction stir processing [5].

Thermo mechanical effected zone is strictly affected by heat and plastic deformation. Metal matrix grains elongate around weld nugget due to insufficient strain energy and heat, recrystallization does not occur in this zone. Sediments dissolution in this zone depends on temperature and time of process, density of lateral boundaries is also high in this zone [5]. Figure 2.15 shows the thermo mechanical effected zone

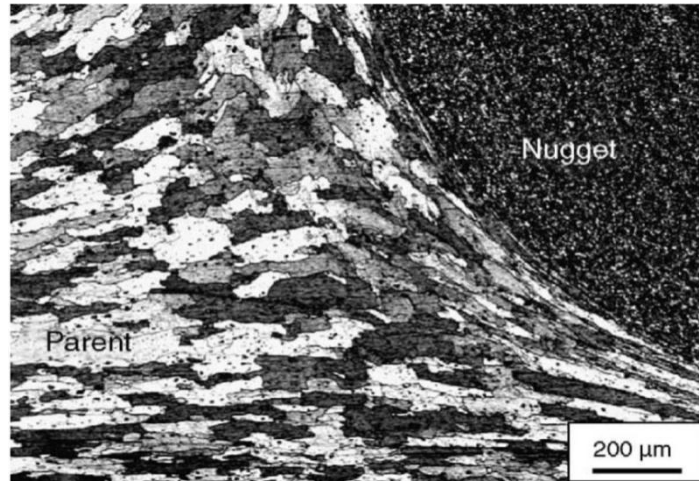


Figure 2.15 Thermo mechanical effected zone7075 aluminium alloy [5]

Thermo mechanical effected zone only experiences the heat generated by the process, no plastic deformation occurs on it. Grain structure of this region is like base metal [5].

Microstructure change is greatly affected by the cooling method and speed of it. For instance about submerged FSP, the final structure has finer grains with compared tothe process done in air. The reason is grain growth limitation during recrystallization[8].Submerged FSP is performed in two methods. in the first method all tool and work piece are under water and in the second method water with determined flow is poured on surface. Figure 2.16 show a picture of submerged FSP [8].

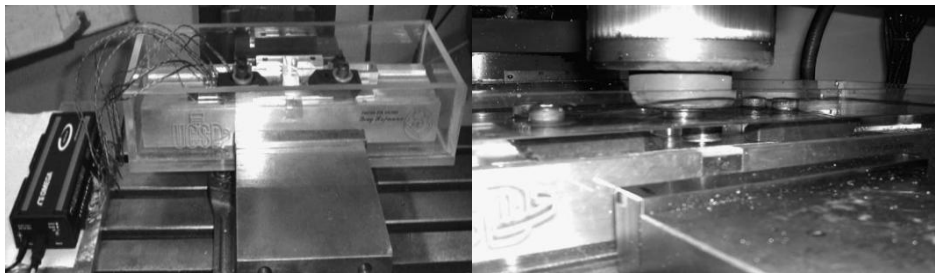


Figure 2.16 Submerged FSP [8]

2.9 Effect of FSP on Mechanical Properties

By applying FSP on casted parts, mechanical properties can be improved greatly. Formed defects during casting wipe out after FSP, also grain size and distribution improve [23, 32, 22]. Particularly when applying this process, creep crack growth ratio reduces. Because surface defects such as oxides which are formed during casting wiped out [22, 20]. Fractography research on AZ91 showed that fatigue fracture forms due to surface oxides holes; Figure 2.17 [22].

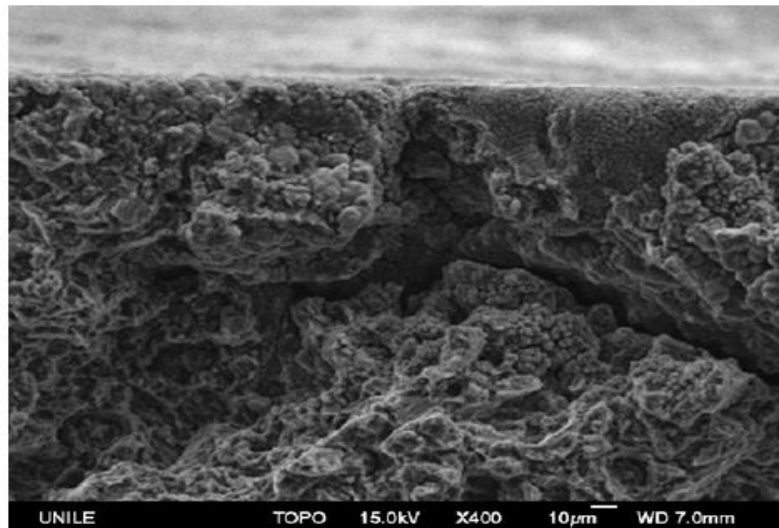


Figure 2.17 fracture plane of AZ91 which indicate the onset of fatigue fracture crack via surface hole [22].

It is clear in Figure 2.17, the structure of AZ31 after FSP, is uniform and no defect is visible. Generally the mechanisms of strengthening the reinforced metal matrix composites with particles are [18]:

- (1) Orowan strengthening
- (2) Grain size
- (3) Hardness due to formed dislocation, because of difference in thermal contraction between reinforced particles and metal matrix.

(4) Work hardening due to strain misfit between elastic reinforcement particles and plastic metal matrix.

According to microstructural characteristics of composites generated by friction stir processing, the main parameters for increasing the hardness of the produced composite layer are (1) fine grains (2) Orowan strengthening due to uniform distribution of reinforcement particles.

According to Hall-Petch equation, there is a reverse relation between hardness and grain size [33]. Relation (2.3) show the general form of Hall-Petch equation where A, k, and α , are constant values and are found by experiment for each material.

$$HV = A + kd^\alpha \quad (2.3)$$

In friction stir processing hardness is increased because of reduction in grain size. Equation (2.4) shows the Hall-Petch equation for AZ31 magnesium alloy.

$$HV = 40 + 72d^{-1/2} \quad (2.4)$$

However in some alloys proceeded by friction stir processing, sediment phases are solved which causes in reducing hardness.

2.10 Methods to Achieve Very Fine Grain Structure

For good mechanical properties very fine structures in many cases are better than coarse structures. Studies have shown that very fine structures form very easily in alloys that have hardness precipitation capability, because sediment and secondary phases particles are stuck in boundaries and lock themselves, hence preventing grain growth [34] there are different methods to refine microstructure and material grain.

But mostly the methods below are used to achieve very fine grain. [35, 32, 7, 34]

- Mechanical methods: rolling in low temperature or pressing
- Severe plastic deformation
- Distillation gas particles
- The electric deposit
- Using grain refiners
- Rapid cooling

Specially, severe plastic deformation done in several method [7, 32]

- applying severe plastic torsion strain
- High pressure torsion
- Cyclic channel die compression
- Friction stir processing
- Equal-channel angular pressing (ECAP)
- Accumulative roll bonding (ARB)

General form of each method showed in Figure 2.18

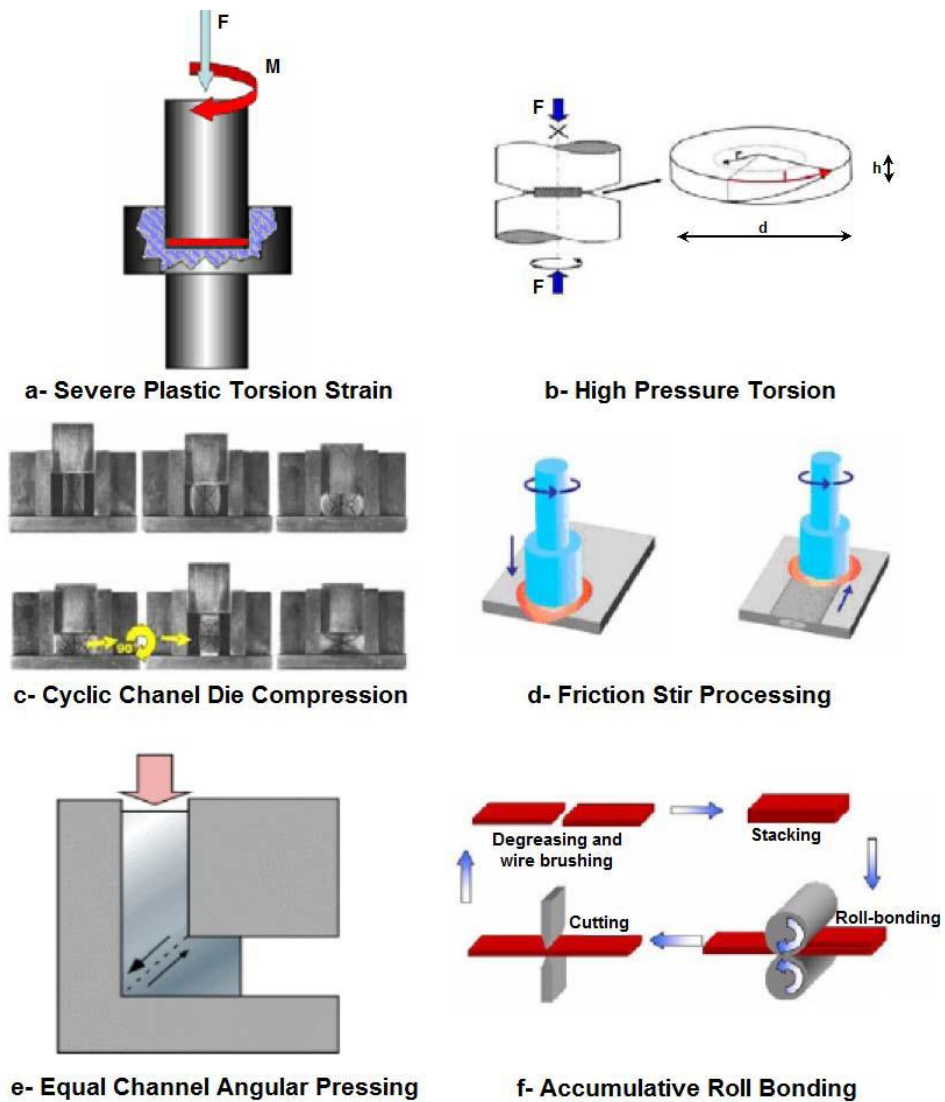


Figure 2.18 Severe plastic deformation methods [35].

The plastic torsion strain method includes applying quick and high changes in torsion on a billet in certain periods and in a specified direction. In high pressure torsion two billets are placed on each other and a high perpendicular force is applied on parts while parts are rotated in opposite direction to each other. This method can be considered as a friction process.

Among all severe plastic deformation methods, equal-channel angular pressing (ECAP) is the most application method. In this method a billet carries intense shear with no change in its dimensions [13] it have been reported that applying two step

ECAP by homogenized process at 413 °C for 19-18 hours causes an improvement in grain structure and also the morphology change from rod elongated beta deposits ($Mg_{17}Al_{12}$) to fine particles [9]. Kim et al [47] also found out in their studies that severe deformation of magnesium alloys in mold edge causes a texture with high Schmid factor to form and because of this difficulty slip strength increased. However after applying this process, the toughness also decreases because the work hardening ability decreases.

In equal-channel angular pressing, a billet with width less than chamber width is placed under pressure and deformed. Then the billet is shifted to another direction and deformed.

The other method is FSP or friction stir processing. In accumulative roll bonding (ARB), a metal sheet undergoes severe plastic deformation. In this method, two metal sheets with same dimension are placed over each other and rolled to 50% reduction in cross section. Then the final sheet gets cut and the operation is repeated again. Via theoretically view this operation can be performed for an infinite number and finally very fine structure can be achieved. It should be considered that in order to obtain good bonds between sheets, before rolling, the surface of the sheets must get cleaned of surface sediments and oxides by using mechanical and chemical methods [7].

In comparison to all plastic deformation methods, FSP give a uniform structure with uniform grain size distribution. In this method there is no sign of non uniform grain growth compared to other methods [34, 32].

Chapter 3

METHODOLOGY

3.1 Materials

An aerospace grade aluminium alloy AA7075-T6 was employed as the experimental material, composition of which is as given below in Table 3.1:

Table 3.1 Chemical combination of aluminium alloy 7075

Si	Fe	Cu	Mn	Mg	Cr	Ni	Zn
0.06	0.18	1.55	0.17	1.4	0.19	0.01	
Pb	Sn	Al	V	B	Bi	Co	Zr
0.01	0.005	Base	0.007	0.002	0.005	0.003	0.002

3.1.1 Properties of 7075T6 Aluminium

AA 7075 because of its low weight and high strength to weight ratio and relative low cost compared to the same level aluminium alloys, is a good alternative to steel because of reduction of structure weight. These properties are mostly required in aviation and military industry. Table 2.1 shows the properties of 7075-T6 alloy.

\

Table 3.2 AA 7075 properties

Property	Value
Machine-ability%	70%
Electrical resistivity	5.15e-006 ohm-cm
Thermal conductivity	130W/m-k
Elongation at break %	11%
Density	2.81 g/cc
Melting point	477-635 °C
Modulus of elasticity	71.7 Gpa
Shear modulus	29.6 Gpa
Crystal structure	FCC

Aluminium alloy 7075 sheet is available in market for doing experiments. After Buying the sheet in 1000×2000×5 mm size and 4 kg weight, using guillotine to cutting This sheet in sample size 120×100 mm, Figure 3.1. One of the important factors to should be considered during cutting process is that, the length of sample, cut in rolling direction of sheet, Because FSP will be done in direction of sample length.



Figure 3.1 Initial shape of work-piece.

To generate composite layer, ceramic powder must be added to operation zone, for this work groove with 1 mm thickness and 2.5 depth machined on the surface of samples. Figure 3.2 shows samples with groove.

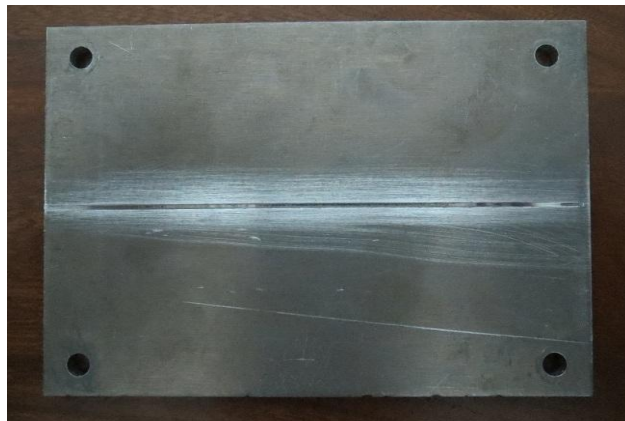


Figure 3.2 FSP Work-pieces with groove.

3.2 Ceramic Powder

To generate composite layer using nitride titanium (TiN) this is ceramic powder, as a reinforcement material. The size of this nano-powder is 30 nm with 99.98% purity.

3.3 Friction Stir Processing Tools

Four tools which produce by hot work steel 2344 used in this process that one of them is without pin and only has shoulder and second one has square pin with 5mm square diameter and 2.5 mm pins height. The third one has, pin with triangular shape, with 5 mm triangular height and the last one has threaded taper pin with 1mm pitch size and 0.5 thread depth. Shoulder diameter in all tools is 15 mm. tools after machining heat treated for hardening. The tools hardening is about 52 ± 2 C Rockwell figure 3.3 show the FSP tools.



Figure 3.3 FSP tools.

After filling slot with TiN powder, to preventing the powder to vent of work-piece during process, surface of slot closed by first tool(without pin tool). The other tools are main tools of FSP.

3.4 Equipment of the Friction Stir Processing

The equipment used in this research is a conventional vertical milling machine which by clamping a fixture on its table, change to FSP machine. The needed fixture designed in way that can fix the work piece on it, so that can prevent movement and sliding of samples under process force. Picture of machine with tool and clamped work-piece in figure 3.4.



Figure 3.4 Machine and fixture used in FSP.

FSP process began with clamping and tightening fixture on milling machine table, and then clamping aluminium sheets on fixture. Slot filled with TiN powder and then compacted. Tool with no pin mounted on milling machine spindle. With turning on the machine and starting rotational motion of spindle, shoulder of the tool gradually tangent to the surface of the work-piece at beginning of slot. And penetrate 0.15 mm in sample then feed applied on machine table. As shown in figure 3.5, after closing surface of groove, the first tool is open from machine spindle and main tool mount on machine.

Then the pin of rotational tool penetrate on work-piece, as far the shoulder of tool penetrate 0.3 mm in work-piece. After nearly 20 second stop to heating the work-piece and make it soft, around the pin, feed movement began and tool move along the groove length.

3.5 Fixed Parameters

3.5.1 Rotational Speed

Rotational speed of tool or rotational speed of spindle which selected 1250 rpm

3.5.2 Feed Rate

Feed rate of table or tool feed rate 40 mm/min selected

3.5.3 Tilt angle

Tilt angle of tool is 2.5 degree

3.5.4 Depth of tool penetration

It measured, where shoulder of tool touch the surface of work-piece, figure 3.5.

Depth of penetration is 0.2 mm

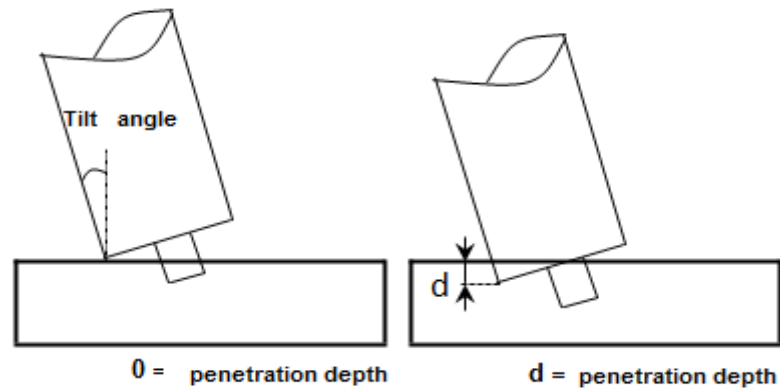


Figure 3.5 General figure of tool penetration.

3.6 Investigated Parameters

3.6.1 Number of Pass

To investigate effect of number of pass on grain size, powder distribution, samples generated with two and four passes.

3.6.2 Direction of tool rotation

Generally the direction of tool rotation is counter clock wise. But to investigate the effect of change in rotation direction in two passes samples first pass is ccw and second pass is cw and in four passes samples first two passes done ccw and the other two passes done cw.

3.7 Metallography

To prepare metallography samples, samples with 32 mm length, perpendicular to welding direction and 4 mm thickness cut from FSP work-piece. Cross section of cut samples sanding with 800 to 5000 mesh, then polished and etched with etching soluble for 15 second.

Figure 3.6 show a etched metallography sample, to investigate microstructure of samples a optical microscope used with 100,200,300,400 magnification, Figure 3.7 show a picture of this microscope

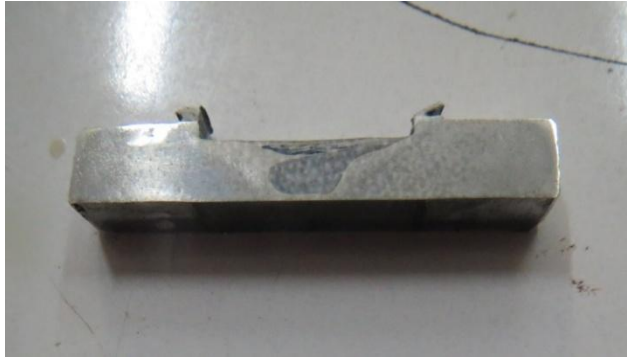


Figure 3.6 Etched, metallography sample



Figure 3.7 Optical microscope

3.8 Tool Geometry

To investigate effect of tool geometry samples prepared with three different shape, square tool ,triangular tool , and threaded taper tool

3.9 Hardness

The etch samples again sanding to remove the etched surface. The micro-hardness(Vickers) testing run in the length of the metallography samples(perpendicular to the tool direction) in center of the sample. Figure 3.8 show the picture of Vickers micro-hardness tester. The applied load in this test was 100 N(HV10) for 15 second. With using the optical equipment and measurment

equipment on the machine the diameter of effected point measured and result displayed on monitor. Figure 3.9 show this equipment.



Figure 3.8 Hardness tester Figure 3.9 Measurement equipment

3.10 Wear Properties

For preparation wear test samples, circular samples with 5mm diameter cut by wire cut machine from center of welding zone. The machine which used for wear test is pin-on-disc machine. Figure 3.10 show the schematic of this machine.

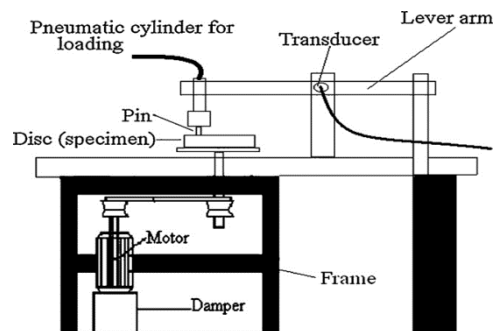


Figure 3.10 Schematic picture of wear test machine

The material of disc used in this experiment is 52100 steel which has 62 RC hardness. The parameters that wear test carry out are 20 N force, 0.5 m/s (364 rpm) rotational speed of disc the diameter of the sample 5 mm, friction radius on disc 13.1

mm the time takes to run each test is 33 minute and 20 second. Figure 3.11 show the picture of disc and the sample, and the regions which samples cut.

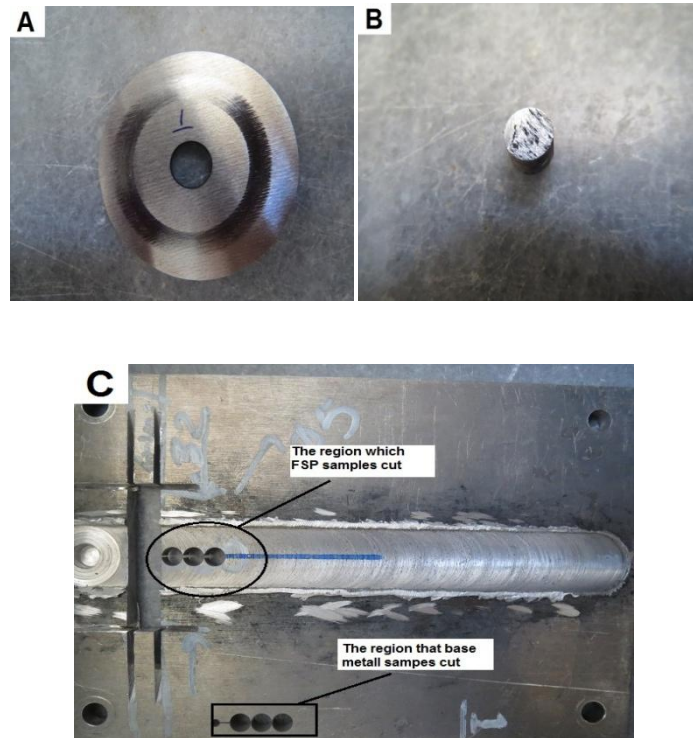


Figure 3.11 (A) show the disc picture (B) is picture of samples (C) show the region of FSP work-piece which wear samples cut

3.11 XRD Test

XRD test was performed on FSP zone in the center of weld nugget in tool feed direction to investigate the generated intermetallics.

3.12 Tensile Test

Tensile test is run in order to determine the (UTS), and (YTS) and elongation percent. Tensile samples cut in the length of the FSP samples from center of the tool welded zone. Figure 4.16 shows the tensile specimen and tensile machine which is used in this test.

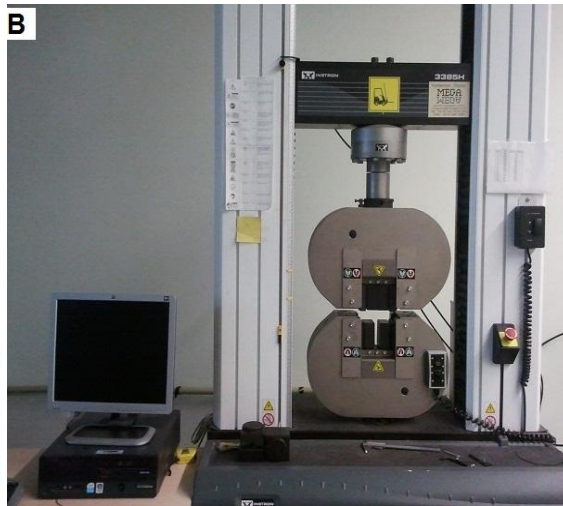
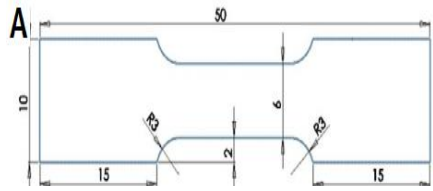


Figure 3.12 Tensile specimen(A) and tensile machine(B)

Chapter 4

RESULT AND DISCUSSION

4.1 Producing a Sample without Defect

Figure 4.1(A) shows the sample surface after covering the surface slot without a pin tool. As it is clear, zone under process is uneven and rough. Figure 4.1(B) shows the surface of sample, after running friction stir processing by triangular tool. In this sample because of turbulence and plastic deformation by the tool's pin, heat is generated and as a result there is softening of material, the smoothness of final surface is higher.

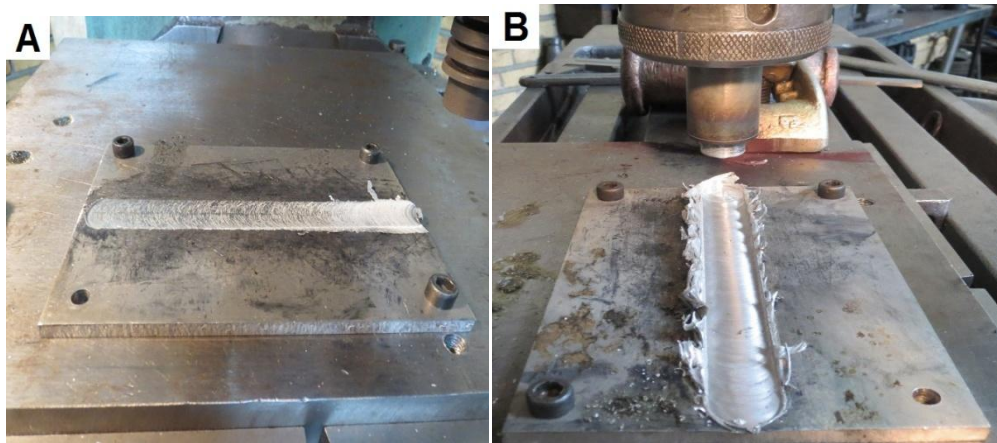


Figure 4.1 Surface of the samples after processing by no-pin tool (A) and tool with triangular pin (B).

4.2 Microstructure

Figure 4.2 shows the microstructure of 7075 aluminium alloy after friction stir processing. In this figure three zone (1) stir (SZ), (2) thermo mechanical effected zone (TMAZ) and (3) base metal (BM) are seen separately.

The average grain size in base metal is 75 μ m. In stir zone the size of the grain reduced more than 30 times. Because of dynamic recrystallization after severe plastic deformation occur in stir zone, grains in this zone are extremely fine and homogenous and final microstructure is generated uniformly. Grains in TMAZ zone, similar to cold forming methods have specific direction that elongated in the stir zone and the base metal zone boundaries. Figure 4.3 shows the microstructure of stir zone and base metal.

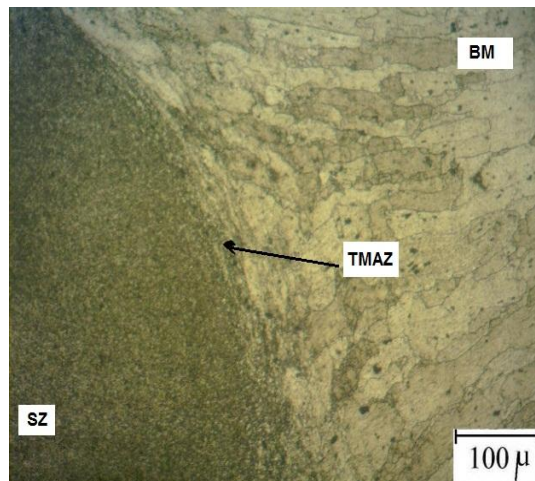


Figure 4.2 The microstructure of BM, TMAZ and SZ

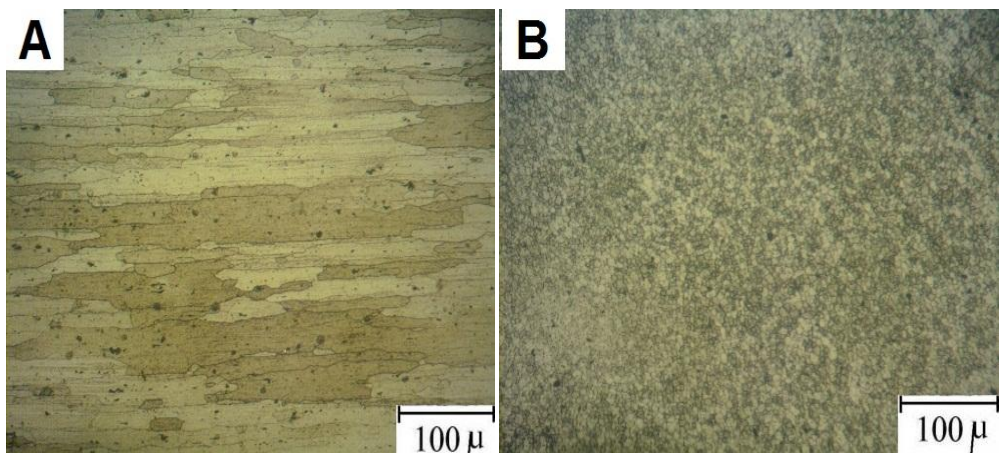


Figure 4.3 Microstructure of (A) base metal (B) stir zone

The amount of temperature and mechanical strain determines the size of TMAZ. Increasing the amount of mechanical strain, causes increase in the width of TMAZ.

The TMAZ in the advancing region (Figure 4.4 A), is narrow and its boundary is apparent with base material and SZ. The TMAZ in the retreating region (Figure 4.4 B) is wide and its boundary is not clear with base metal. In this region, the amount of mechanical strains and generated heat is more than in the advancing side. In this region as one move from SZ to the base metal, elongation of grains reduces and their distribution increases.

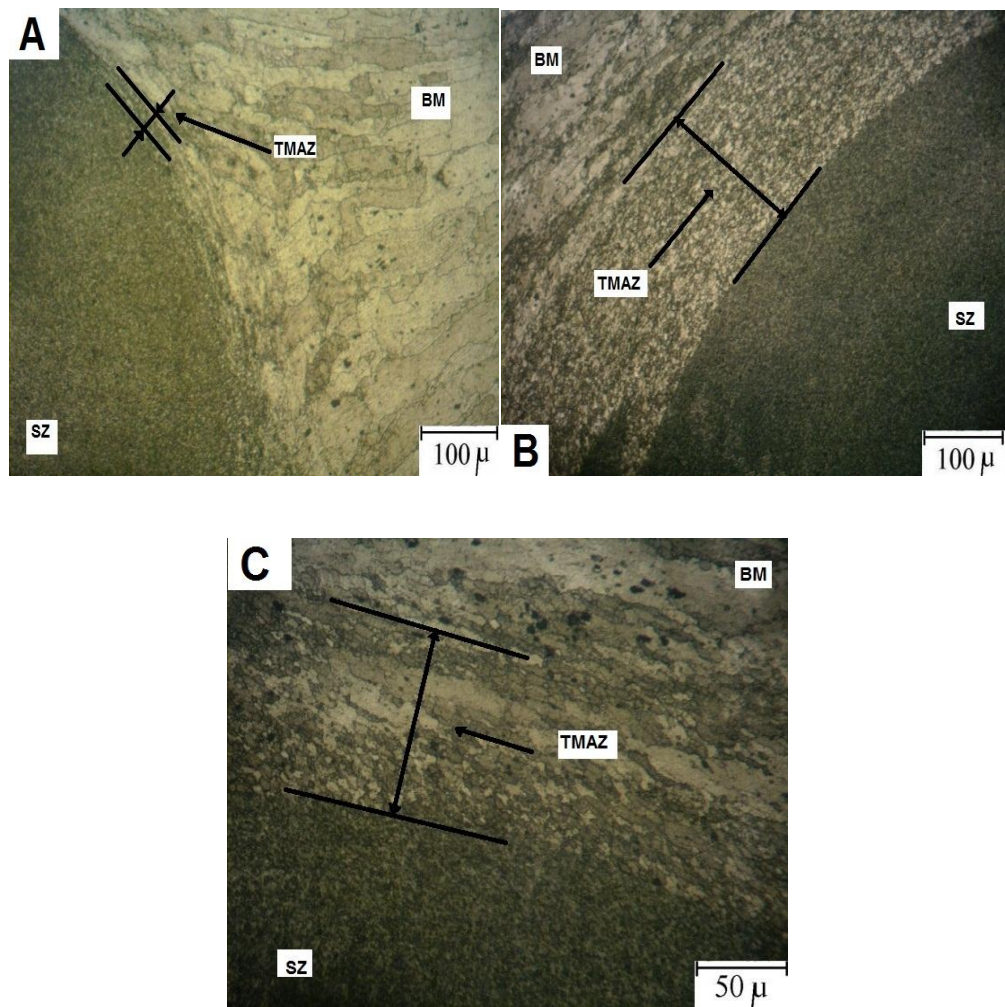


Figure 4.4 (A) advancing TMAZ, (B) retreating TMAZ, (C) downward TMAZ

In the TMAZ (Figure 4.4 A, B) the tool's pin has linear contact with base material whereas in downward TMAZ the tool's pin has planar contact with base metal as a result of amount of plastic deformation and mechanical strain in downward TMAZ is higher and grains are elongated and compressed with each other.

4.3 Producing AL 7075/TiN Nano-Composites

After machining the groove 2.5 mm×1 mm on the surface of the samples and filling it with TiN nano-powder, the surface of the slot is covered by a tool with no pin and FSP is done by the second tool. Because of mechanical turbulence TiN particles are distributed in base aluminium.

Figure 4.5 (A) and (B) show the microstructure of SZ in FSP samples with 30 nm TiN powder. As can be seen in Figure 4.5 the size of the grains in the region that has a good distribution of nano-powder (A) is finer than where the distribution of powder is not good (B). In fact because of TiN particles pinning the growth of grains during recrystallization is restricted. By reducing the nano-powder particles size, the pinning is better.

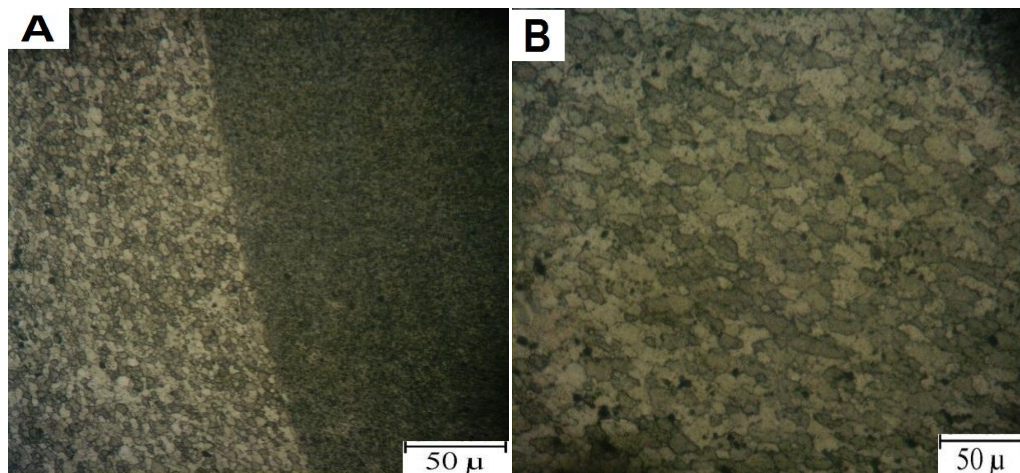


Figure 4.5 Microstructure of FSP zone with good distribution of powder (A) and no good distribution (B).

Result of EDS analysis over white point which is shown in Figure 4.6, shows that white points in this figures are TiN.

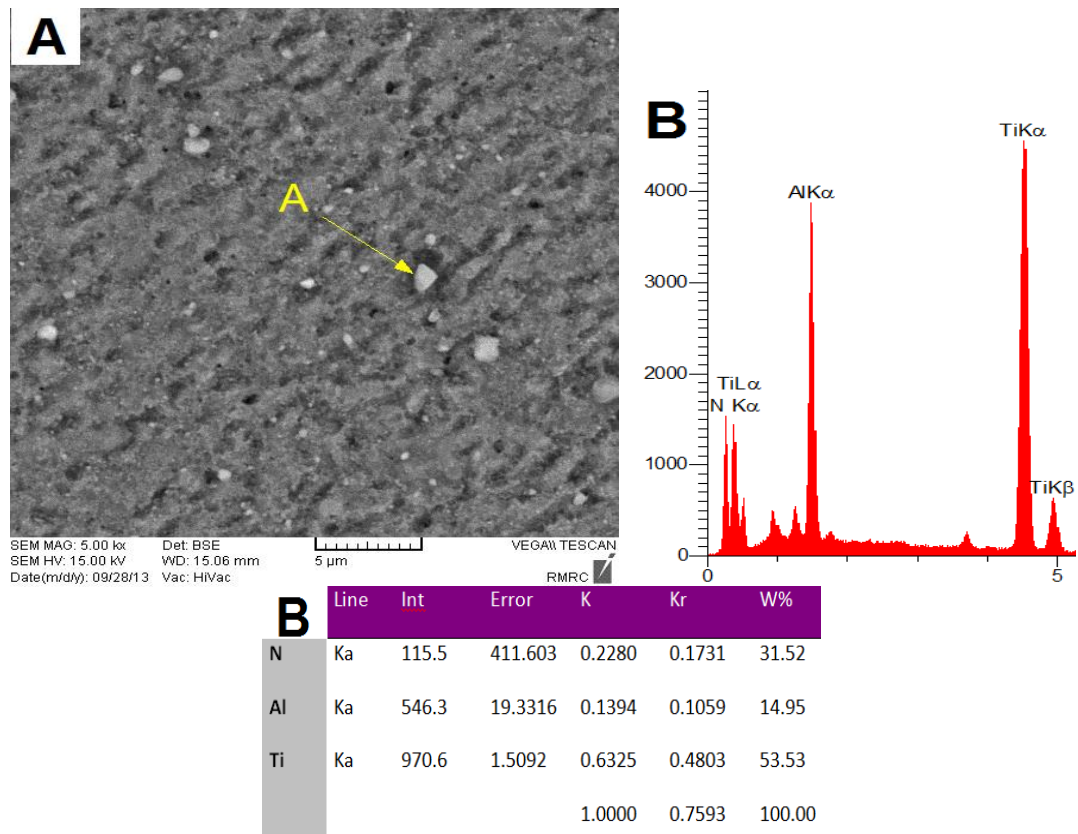


Figure 4.6 (A) SEM picture of SZ zone and (B) shows EDS analysis result of white point.

Distribution of TiN powder in aluminium matrix is not uniform. In some FSP samples nano-powders cumulates on some regions. Figure 4.7 shows an OM picture of the SZ zone, where the nano-powder cumulated.

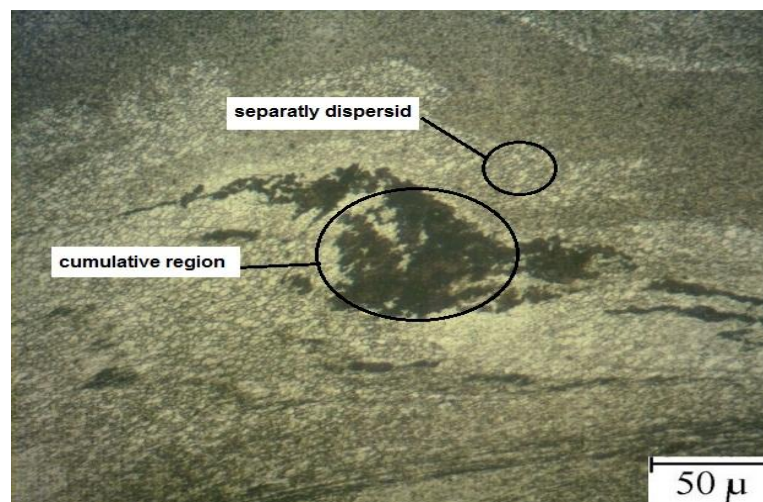


Figure 4.7 OM picture of cumulative region in stir zone

Generally, in FSP samples two regions are generated. (1) The region in which the TiNnano-powder is distributed with high density. (2) The region in which TiNnano-powder is distributed with low density.

Figure 4.8 (A) shows a picture of a 4 passes FSP sample section. The bright zone is the region with high nano-powder density and the dark zone is region with low nano-powder density. Picture (B) and (C) show the microstructure of dark region and bright region respectively.

Distribution of TiNnano-powder in bright region is never uniform and strips like flames are generated in the advancing side, which in fact show the flow of material in SZ. Figure 4.8 (D) and (E) also show these strips in bright zone.

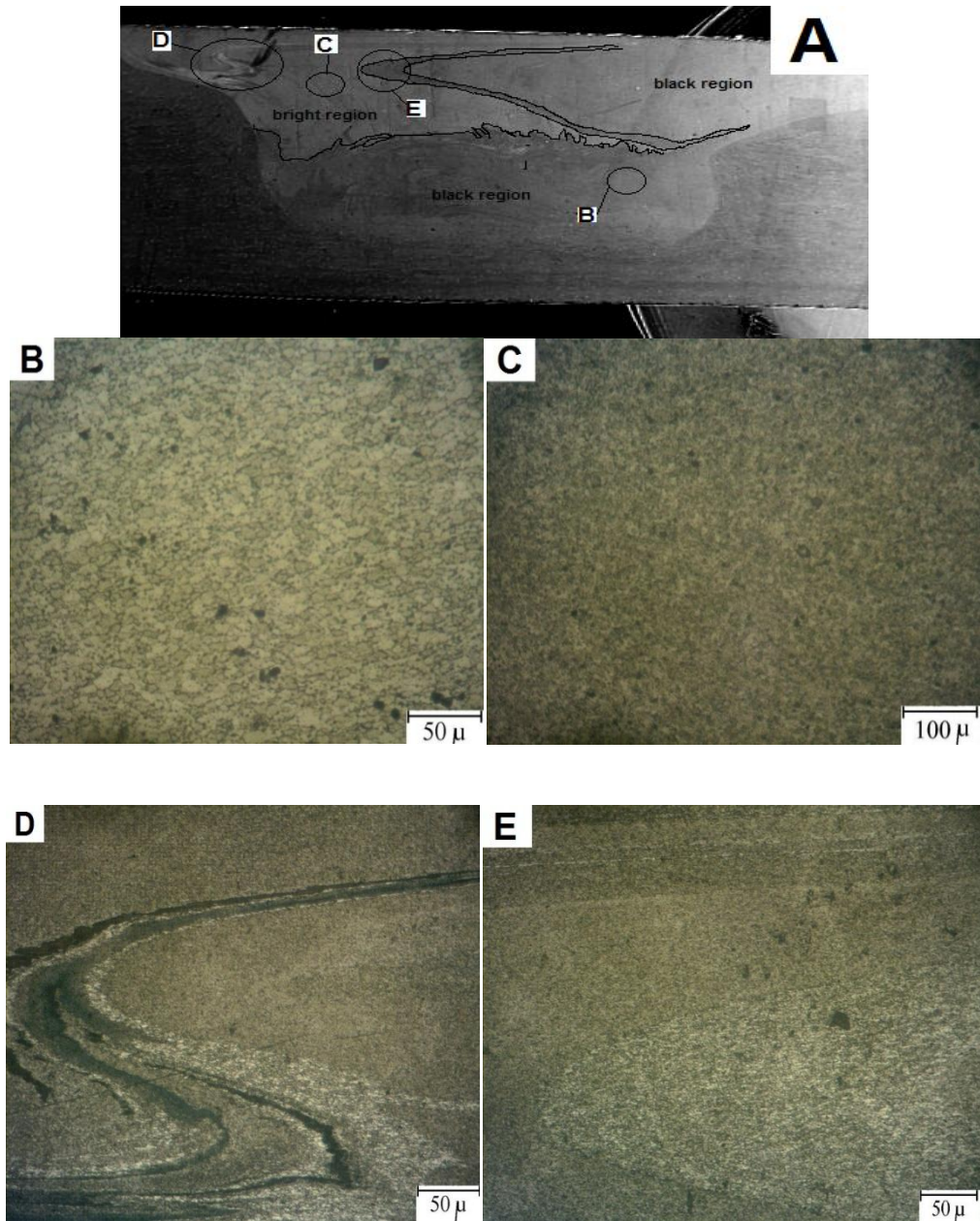


Figure 4.8 (A) SEM picture of FSP sample (B) to (E) microstructure of showed regions in (A)

4.4 Effect of Number of Pass on Process

4.4.1 Effect of Number of Passes and Tool Geometry, Direction of Rotation on Micro and Macro Structure of Samples

As mentioned, the distribution of the nano- powder in the stir zone is never uniform and creates two dark regions with low density of powder and a bright region with high density of powder. Figure 4.9 shows the effect of pass number and change in

direction of the tool rotation on powder distribution. In two pass samples (A),(C),(E), which were produced respectively by triangular tool, square tool and threaded taper tool, the nano-powder is distributed with high density only in a small region of the advancing side(A) and the downward SZ(E),and there is a narrow strip of cumulative powder in nugget of the weld near the surface (E) , this means in the two pass samples the nano-powder is distributed non-uniformly.

in four passes samples (B), (D), (F) which made by triangular tool, square tool, and threaded taper tool respectively, by increasing the number of passes, the nano-powder was distributed in wide district whereas there is no sign of cumulative powder in these samples and also only a narrow dark strip that can be observed in retreating Side (F) and in weld nugget (D).

Since in all samples in each pass, the direction of tool rotation changes, the material flow pattern during mechanical turbulence by pin changes and causes better powder distribution in the stir zone. The effect is much clearer in four passes samples.

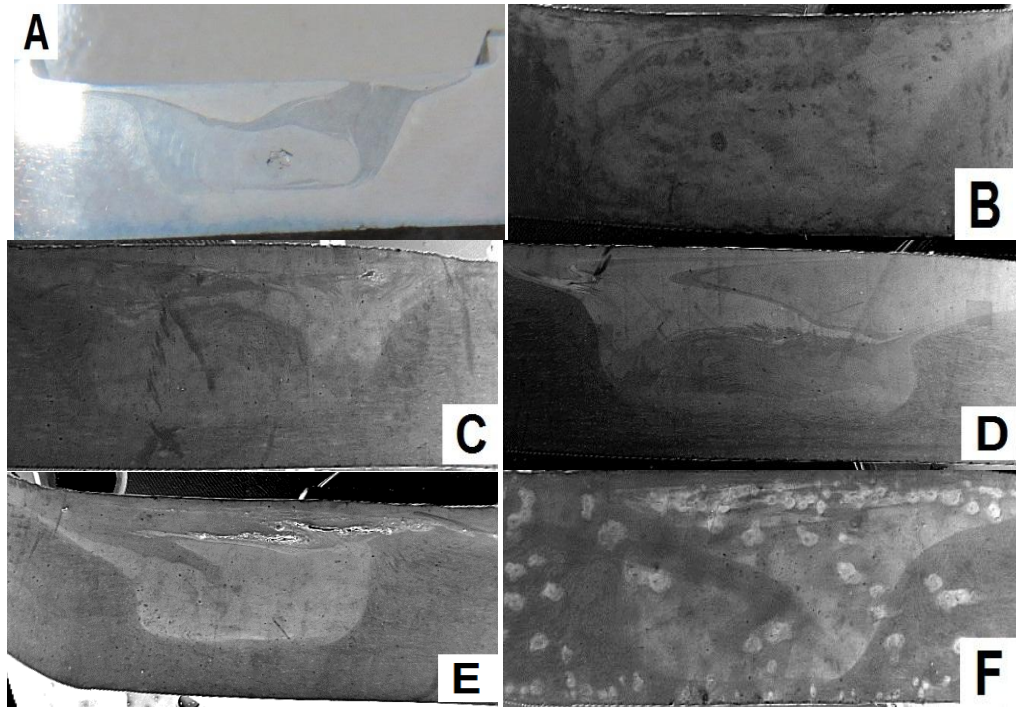


Figure 4.9 Two passes samples (A), (C), (E) and 4 passes samples (B), (D), (F)

Figure 4.10 shows the microstructure pictures of regions which are similar to flames (the narrow strip of base material which flow in to the SZ). (A) Shows the microstructure of FSP sample generated by square tool in two passes and (B) shows the microstructure of FSP sample generated by same tool but in four passes. (C) Shows the FSP sample produced in two passes by triangular tool and (D) shows the sample produced by same tool but in four passes. (E) Shows a picture of the sample generated by threaded taper in four passes.

By comparing these pictures it can be seen that the difference in size between the fine and the large grains in two pass samples is higher than four pass samples.

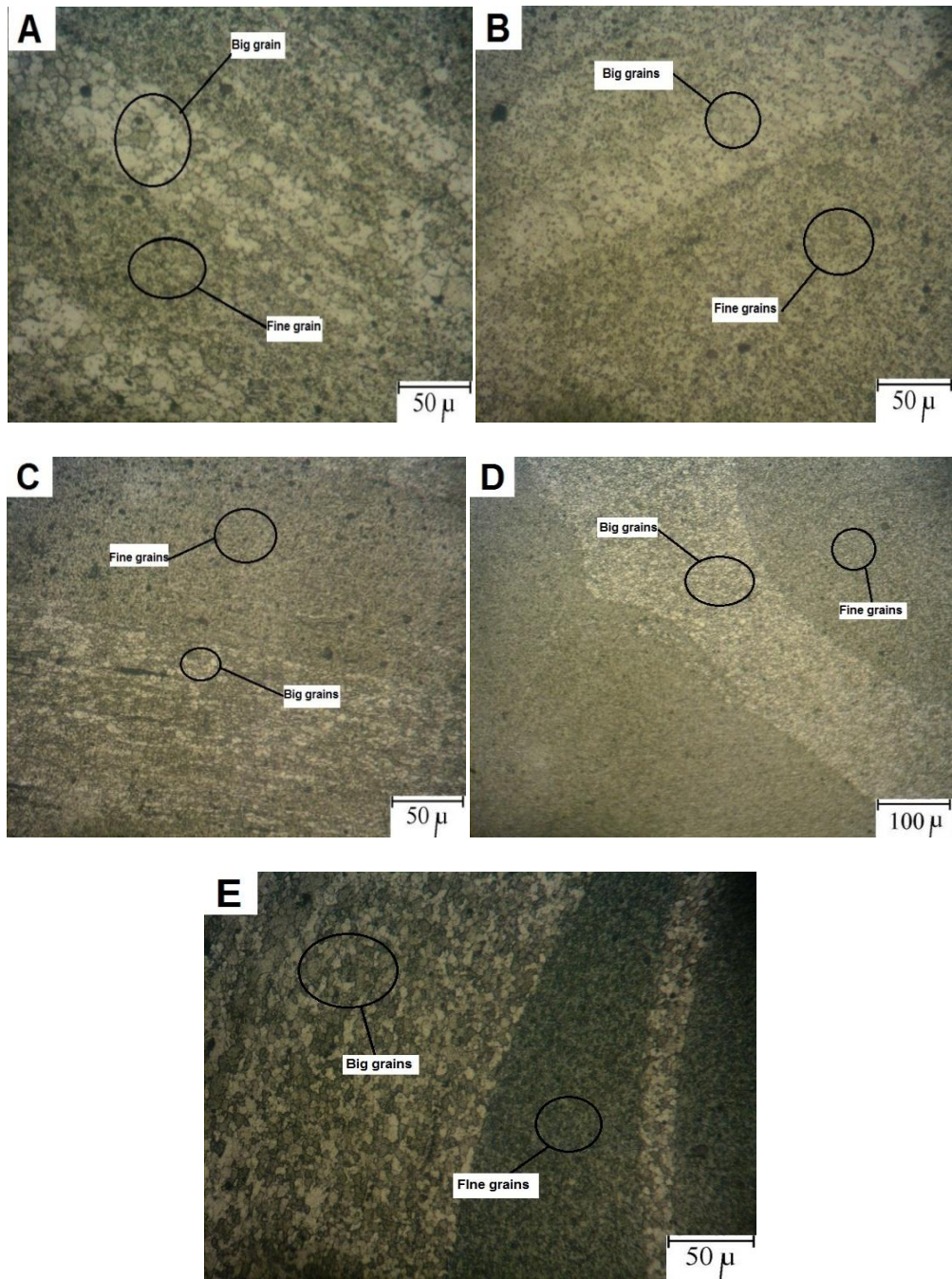


Figure 4.10 Size difference between fine grains and large grains in different tools

Increasing the number of passes in the process causes grain size reduction because of two reasons: by increasing number of pass(1)the bright area which include high density of nano-powder increase (2)the grain size in both dark and bright regions decrease because of recrystallization happens in each new pass.

Figure 4.11 shows the effect of tool geometry and pass number on the microstructure of FSP samples. Grain size of each sample is written under its picture. The finest grain size belongs to threaded taper tool followed by triangular tool then follow by square tool samples. Increasing the number of passes to four, does not show a significant change on grain size of samples compare to two passes, but selecting low feed rate and high rotation speed cause a rise in temperature and as a result higher grain growth in four passes.

In four and two pass samples differences normally occur due to dimensional deference in the width of bright region. On the other hand a change in the direction of rotation of the tool may cause finer grain size. Table 4.1 shows the grain size value for different tool geometry and pass number. Initial grain size of experimental material is 75 μm .

Table 4.1 Grain size values for different tool geometry and pass number

Tool geometry	Mean grin size (Two passes)	Mean grain size (Four passes)
Threaded taper	2.15 μm	1.4 μm
Triangular	2.4 μm	1.86 μm
Square	3.1 μm	2.4 μm

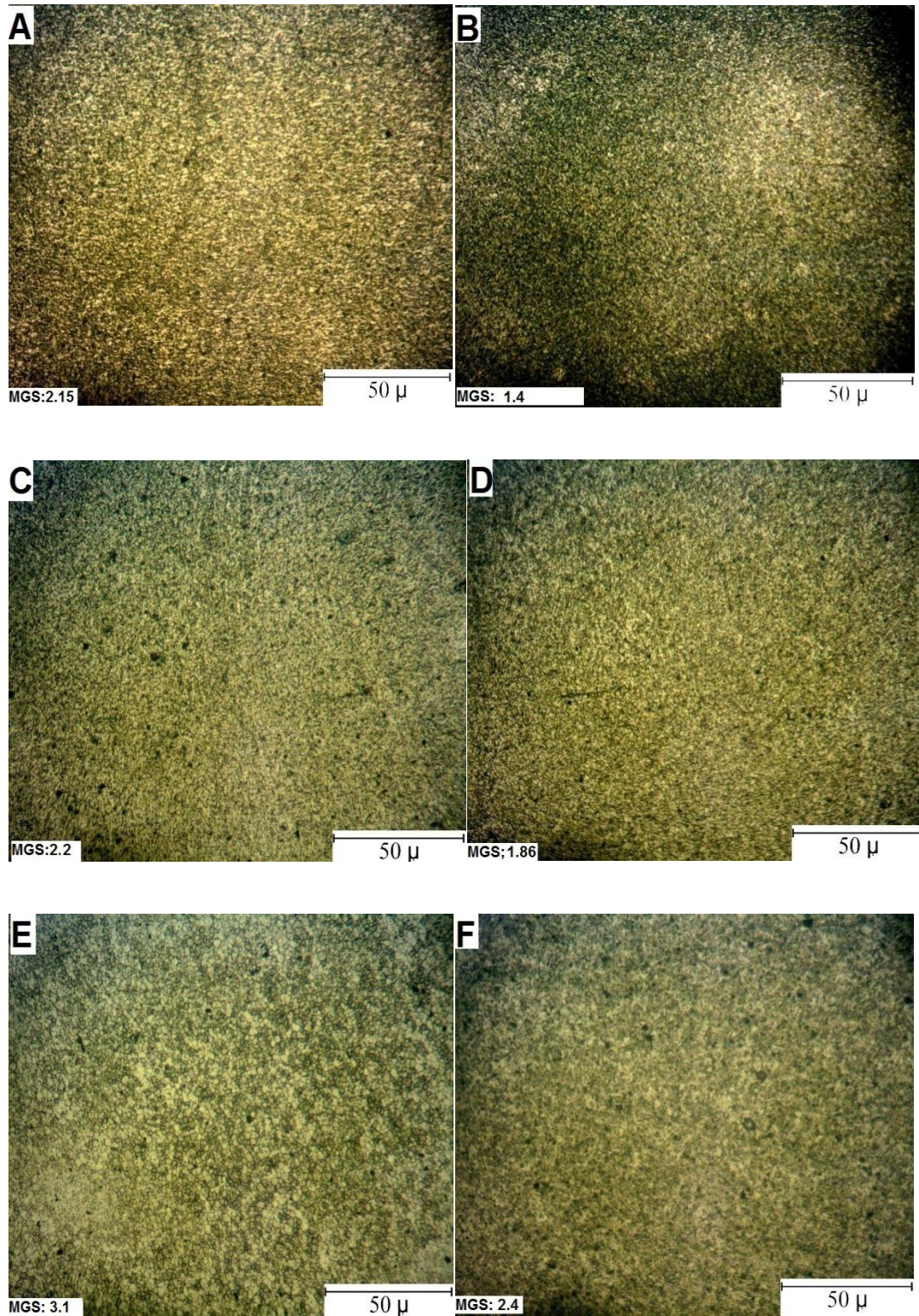


Figure 4.11 Shows OM pictures of SZ; (A)(C)(E) show the two pass generated samples and (B)(D)(F) show the four pass generated samples, also (A)(B) and (C)(D) and (E)(F) show the threaded taper, triangular, and square tool samples respectively.

Figure 4.12 show the SZ, SEM picture of samples produced in four passes by threaded taper tool (A), square tool (B), and Triangular tool (C), with this magnification the distribution of TiN white particle in to the grain is completely observable, which may can be the reason of bounding of nano-powder with base metal.

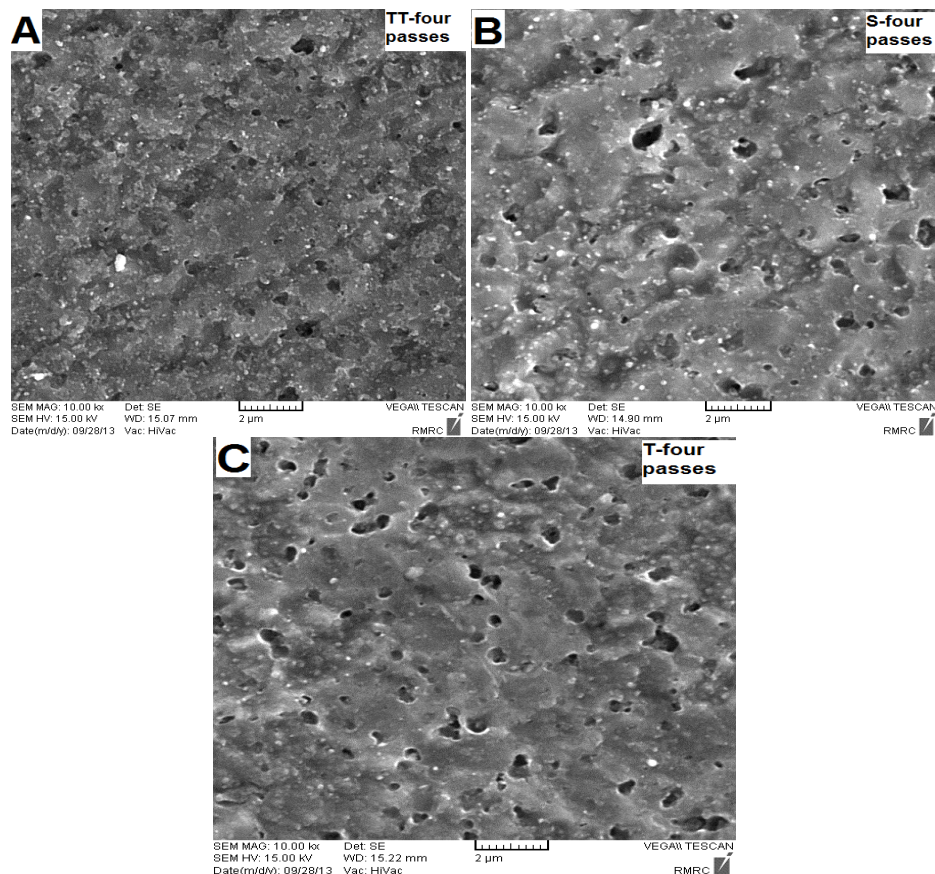


Figure 4.12 SEM picture of stir zone

4.5 Effect of Tool Geometry in the FSP Process by Analyzing Mapping Pictures

In figure 4.12, (A) represents (threaded taper tool), (B) represents (square tool) and (C) (triangular tool) sample SEM pictures of the advancing side produced by four passes of the FSP. The red color shows the Titanium element, green shows the Nitride element and the blue color shows the aluminium element which is the base

metal of the work-piece. In this figure, by studying the threaded taper sample pictures, (D) and (G), it is clear that the Ti and N elements have high density distribution compared to square tool sample pictures,(E) and (H) and triangular tool sample pictures (F) and (I). Also the distribution of Ti and N element in all TMAZ and HAZ zones of the samples observed show thatthere is distributed nano-powder in these zones but this distribution in threaded tapper tool sample is higher than other samples and in the square tool sample it is higher than triangular tool sample. the reason of this phenomena can be explained by the high density of nano-powder in advancing side of threaded taper tool sample.

In figure 4.13 (J),(K),and(L) pictures show the distribution of Ti particles on aluminium matrix respectively for threaded taper, square and triangular tools. It is also clear from picture (D) that high density of nano-powder stops the grain growth during recrystaization (the black space in this picture is smaller than other pictures). From the black spaces which exist in all the pictures, the boundary of grains can be determined by linking the colored dots to form the boundaries and considering the blank spaces as the grains. In samples with high density the spacing between the dots are smaller than other pictures.

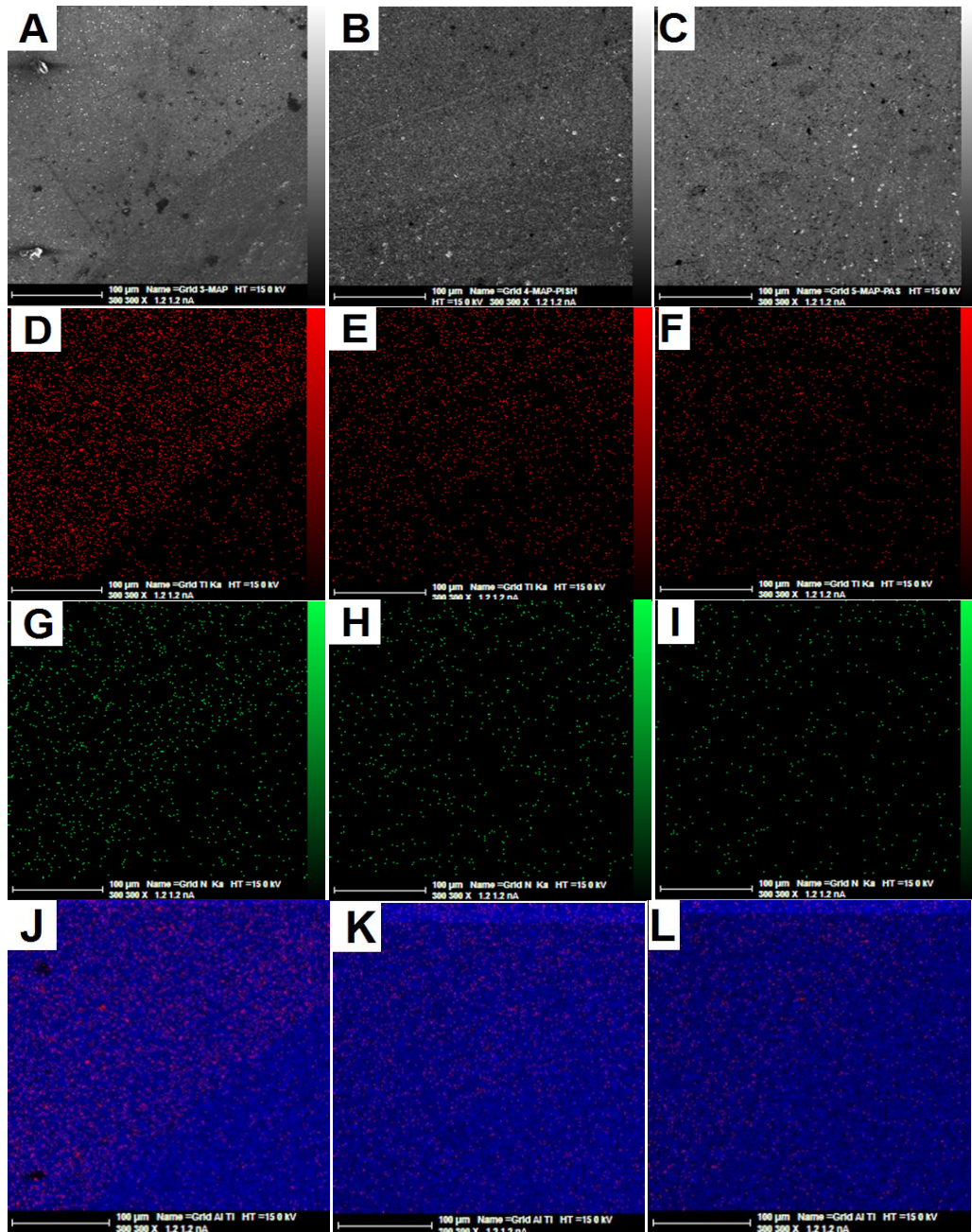


Figure 4.13 shows the mapping of nano-powder in advancing side of samples generated by four pass parameters. (A),(D),(G),(J) pictures belong to the threaded taper tool,(B),(E),(H) and (K) are for square tool and(C),(F),(I)and (L) represent triangular tool pictures

Figure 4.14 shows the SEM pictures (A), (B) and mapping pictures of nano-powder density distribution in the retreating side of FSP sample produced in four pass by square tool,(C),(E),(G) and triangular tool (D),(F),(H),these samples are same samples in figure 4.13. By analyzing these pictures it is understood that the density of Ti and N element in the square tool FSP sample is higher than the triangular FSP

sample, the square tool also has homogeneous nano-powder distribution in the retreating side of sample compared to the triangular tool (there is small a zone of non- homogenous nano-powder distribution). By comparing mapping pictures of the advancing (figure 4.13) and retreating side (figure4.14), it is recognized that in all samples, the density of the distributed nano-powder in the square sample in the advancing side (E),and (H) is lower than the distributed powder density in the retreating side(C) and(E),but in the triangular FSP sample this comparison show that nano-powder distribution in advancing side (F) and (I) and retreating side (D) and (F) are equal.

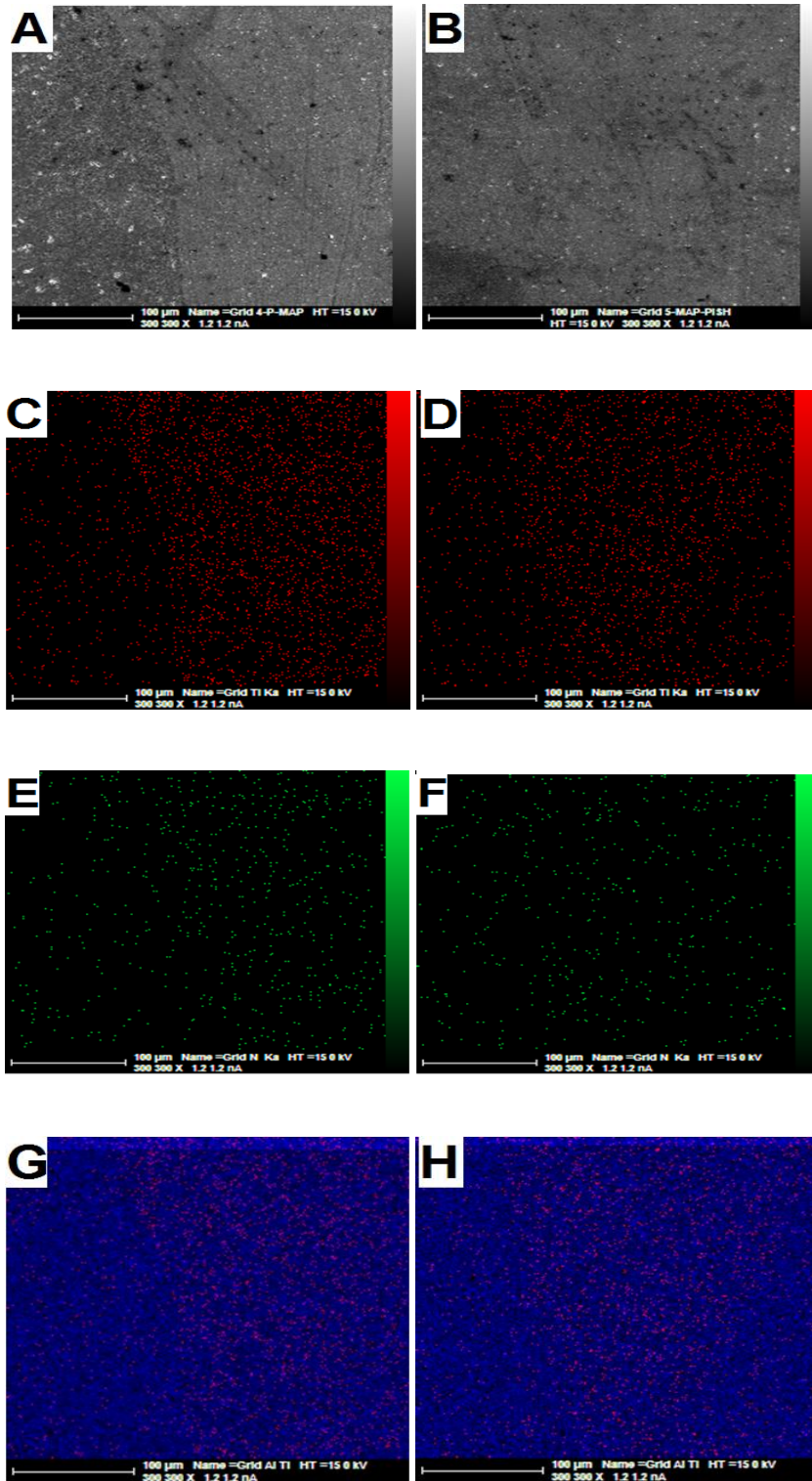


Figure 4.14 Shows the nano-powder distribution in the retreating side of four pass samples ,for the square tool (A),(C),(G),(E) and for the triangular tool (B),(D),(F),(H).

4.6 XRD Analysis of FSP Samples

This part presents the XRD analysis results of FSP samples which are taken from SZ. By studying these data, the existence phase and their amplitudes in each sample are clear. Figure 4.15 shows, the triangular tool, two passes (A) and four passes (B) produced sample XRD graphs. (C) and (D) graphs belong to samples produced by square tool in two and four passes respectively. Graphs (E) and (F) show the results which belong to samples produced by the threaded taper tool in two passes and four passes.

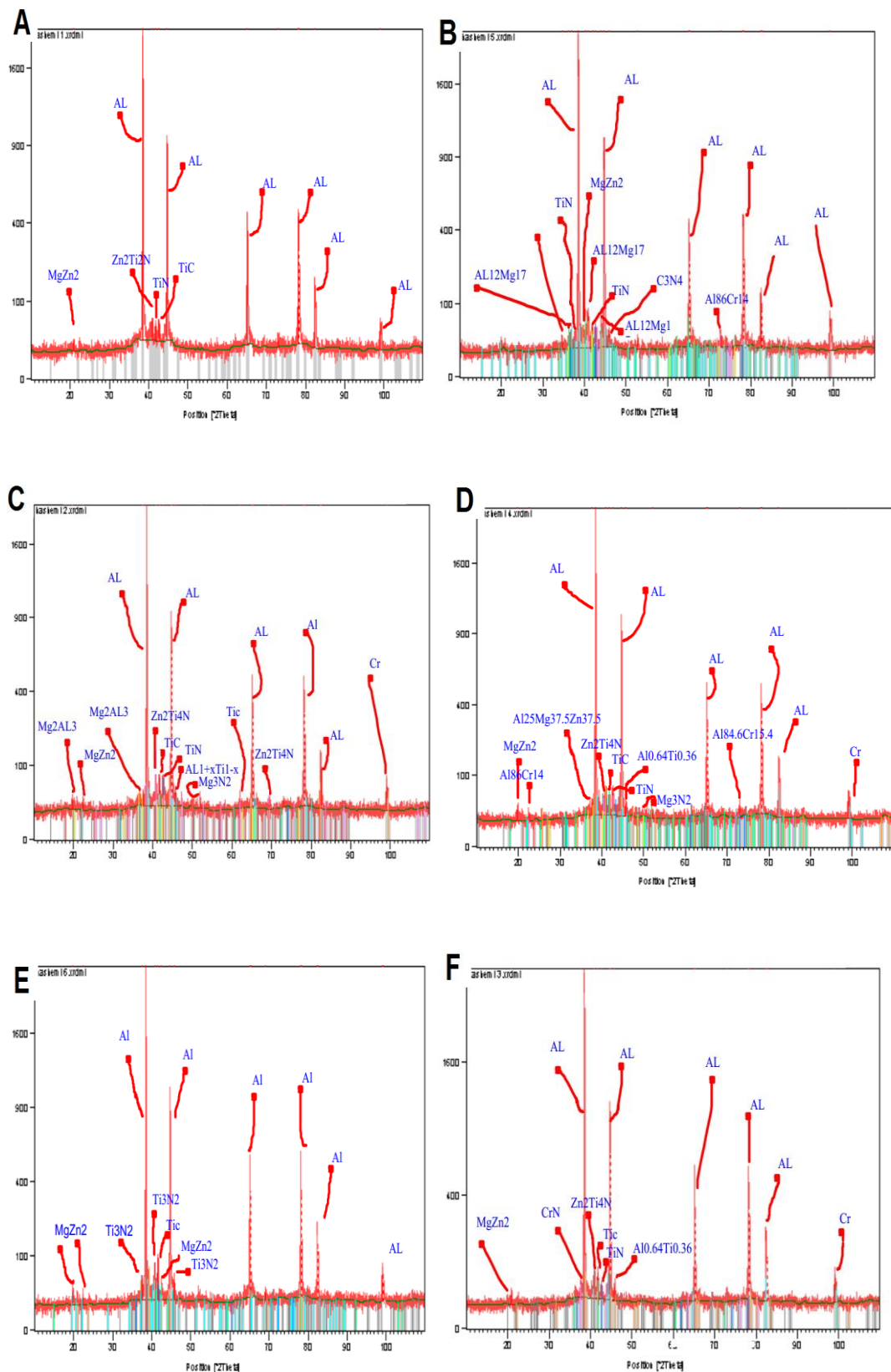


Figure 4.15 The XRD results of samples

As the base metal is AL it is obvious that the high peaks belong to the aluminium and because of TiN nano-powder the peaks belong to this powder in each graph. The important peaks in these graphs are the peaks which show any combination between nano-powder TiN and 7075 Aluminium.

By studying the spectrometry result of the base material (chapter 3 table 4) it is clear that there is a negligible amount of Ti element in base metal (0.01) before FSP and there is no sign of N element in base metal, this means any combination between Ti and N element with other elements is the result of FSP process on 7075 Aluminium. By considering this, the TiC combination in all of samples, Zn₂ Ti₄ N composition in (A),(C),(D) and (E) graphs and Cu Ti composition in (A) and (E)graphs, the peak show the CrN composition is in (F) graph. Mg₃N₂ composition pick is seen in (D) graph and C₃N₄ composition in (B) graph. These results show TiN has good solid solubility in AL and because of high electro-negativity of AL and its trivalent specification; many intermetallic phases are generated in Aluminium.

As is mentioned the FSP process causes localized heating 0.6- 0.9 of the melting temperature. Increasing the temperature causes the reaction between alloying elements and perhaps the reason of existence of intermetallic phase in some samples, because of the difference in heat generated by different tools as other effective parameters fixed in this experiment. The existence of TiN peaks in the graphs is misleading because there is no reaction between alloying elements, however some particles of TiN react with AL 7075 and produce intermetallic phases.

4.7 Mechanical Properties Tests

4.7.1 Wear Test (of FSP Samples)

The parameters which are measured in this experiment are the mass of the pin and disc before and after running test by calculating the mass reduction for each sample and disc. Also this test gives the frictional change in distance for each sample as a graph, and the mean friction coefficient for each sample. Table 4.2 lists results regarding mass reduction and mean friction coefficient.

Table 4.2 Mass reduction of pin, disc, and mean friction coefficient for each sample

Sample	Mass reduction of pin (gr)	Mass reduction of disc (gr)	Mean friction coefficient
Base	0.0041	0.0034	0.59
Triangular (II passes)	0.0035	0.0057	0.66
Square (II passes)	0.0024	0.0039	0.56
Threaded taper (four passes)	0.0019	0.0023	0.48
Square (four passes)	0.0019	0.0024	0.55
Triangular (four passes)	0.0027	0.0045	0.6
Threaded taper (II passes)	0.0031	0.0032	0.69

Figure 4.16 shows the changes in the frictional coefficient during sliding over the distance for each sample. Graphs (A), (C) and (E) show two passes samples produced by triangular, square, and threaded taper tools respectively. Graphs (B),(D),and (F) show the graph of the samples which are produced in four passes by triangular, square, and threaded taper tool respectively; And (G) shows the frictional coefficient change to distance for base metal. The best mean frictional coefficient

value is observed in four passes threaded taper tools samples followed in four passes square tool sample then in two passes square tool sample, other samples friction coefficient are less than the base metal which is due to low density of the nano-powder on the surface near the region in the samples, which is observable in Figure 4.9. In all the graphs, there is an initially rapid elevation of frictional coefficient value in the beginning of sliding recognizable which occurs due to sticking of the sample to the sliding disc and this rapid increase after a specified distance is stable due to generation of some oxide abrasive in the sliding surfaces, and in some cases like (G) till the end of distance stay constant. Sudden fluctuations in graphs may be due to sticking of alloy from sample to disc surface (B).

Generation of an oxide layer can cause a reduction of contact surface and as a result friction coefficient reduction. After a distance, elevation or falling of the graph is observed and may continue for a distance. The reason may be because an abrasive composite layer with low density of TiN or with high density in elevation or in falling the frictional coefficient value respectively. The reason for elevation of the frictional coefficient during the test is due to detachment or break of oxide layers and strengthened surface layers under high stress.

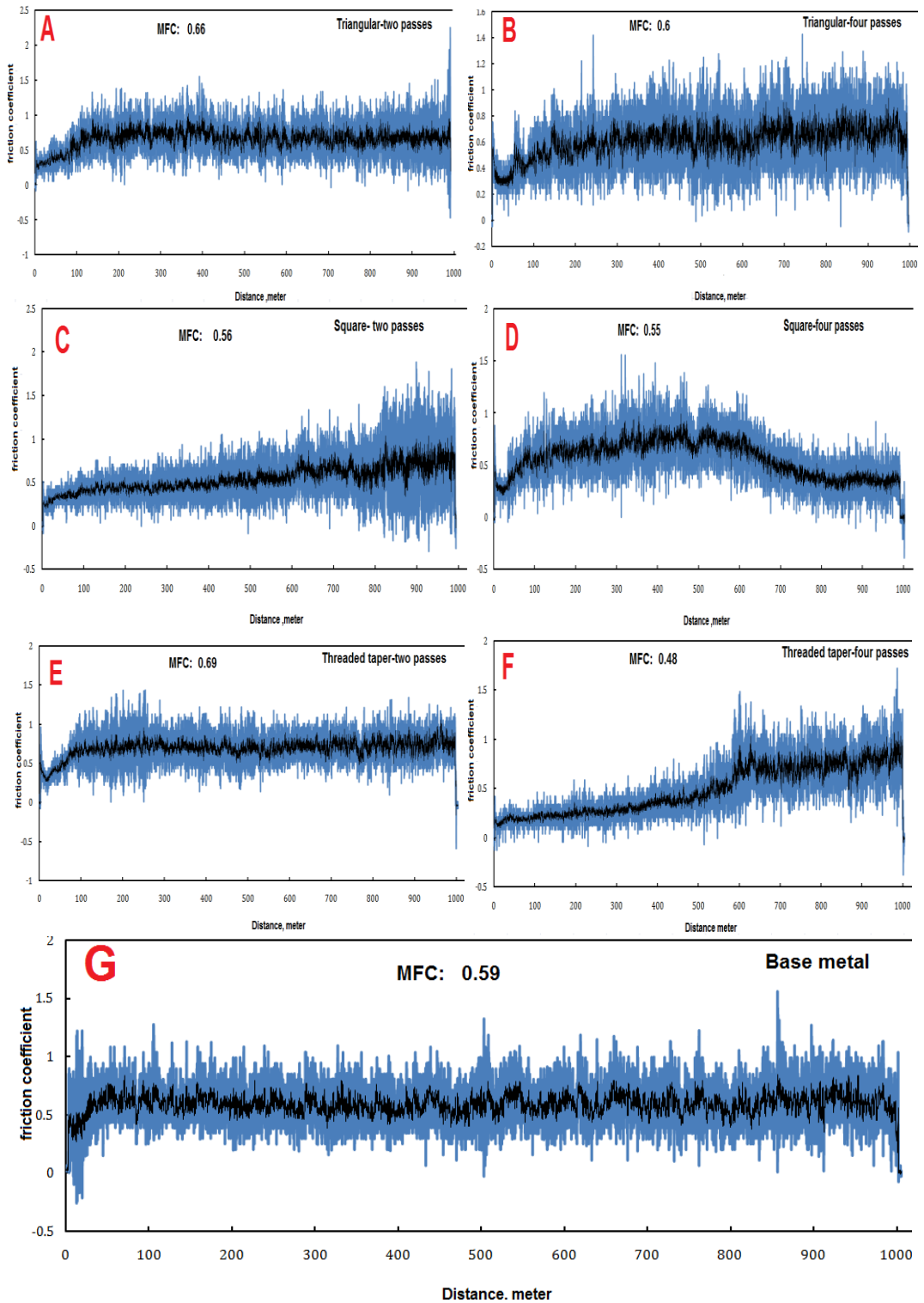


Figure 4.16 Friction coefficient change in distance graphs for all samples

After studying the result of mass loss of pins, it is clear that the biggest amount of mass reduction belongs to the base material, and all other samples with composite and nano-powder show less mass reduction compared to base material, this mass loss, depends on the, number of passes and toll shape variety.

The smaller mass loss of pin belong to threaded taper tool followed by square tool and then the triangular tool samples which are made in four passes FSP; and square tool followed the threaded taper tool then the triangular tool samples which made in two passes FSP. This result shows that by increasing the number of passes from two to four the wear properties of composite elevate. This also shows that the samples which are made by the threaded taper tool and square tool have better wear properties compared to triangular tools; additionally the elevation of wear properties show the excellent metallurgical bounding between nano-powder and base metal.

By studying the disc mass reduction it is clear that the lesser the mass loss measured in the discs, the lesser the mass loss of pin recorded on them. The meaning of this fact is that by increasing the wear properties of pin the wear in disc decreases. By understanding this fact, analyzing wear phenomena between disc and pin is easier.

Strength plays a very important role on wear resistance; In all wear condition an oxide layer is generated on surface of the disk and pin which protects the surface from wear, this can be a reason for an increase in the wear properties of the pin sample and disk simultaneously; also when the material became tougher its wear will be harder than, when it is brittle.

Figure 4.17 shows the macrograph SEM pictures of pins and disc wear surface, in all pins the sliding direction is recognizable by shallow and parallel grooves, figure 4.18 show the SEM picture of one pin and disc and EDS of some point to determine the addition element on the sample due to wear. EDS analysis from point (A) show the existence of ferric-oxide and aluminium-oxide elements, and EDS of point (B) show that white point is ferric, additionally some data in figure 4.19 show the same result from disc wear surface; these oxide elements are one of the reasons for increased wear properties.

Sliding between the disc and pin cuts off layers between the contacting surfaces. The particles from these layers become finer as the process goes on and are distributed by the force applied over the wear surface and decrease the depth on which wear can occur causing a decrease of wear; In the current study these cut off layers contain TiN elements which have superior wear properties and EDS analysis in figure 4.17 from pin wear surface and disc surface in figure 4.18 (B) show the existence of this element (TiN and ferric oxides). Additionally, previously mentioned properties of TiN, high thermal strength of TiN cause the generation of more continuous oxides and increases the covering percent which is one of main reasons which increases the wear properties in FSP samples.

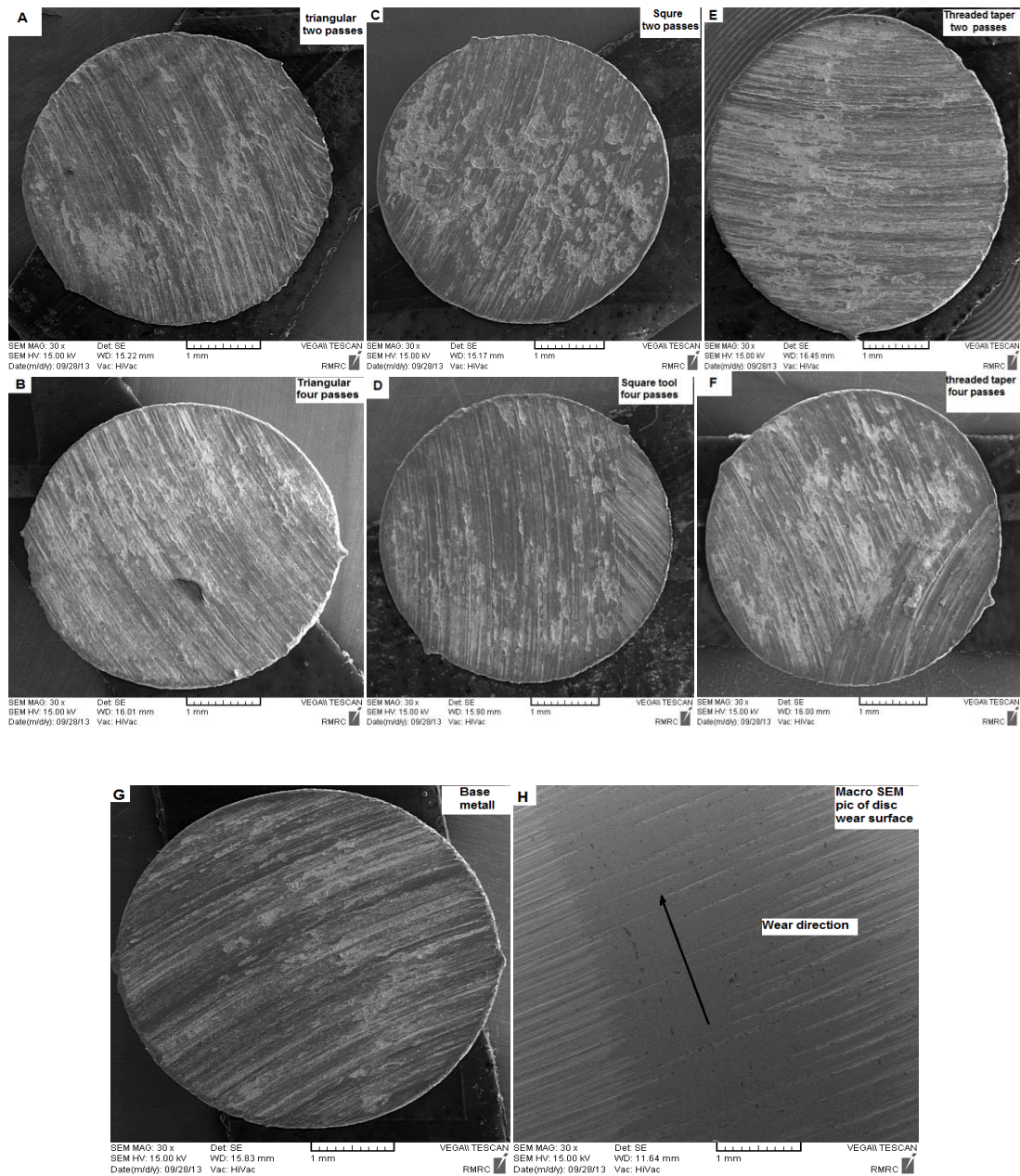


Figure 4.17 Macro pictures of pins and disc wear surface

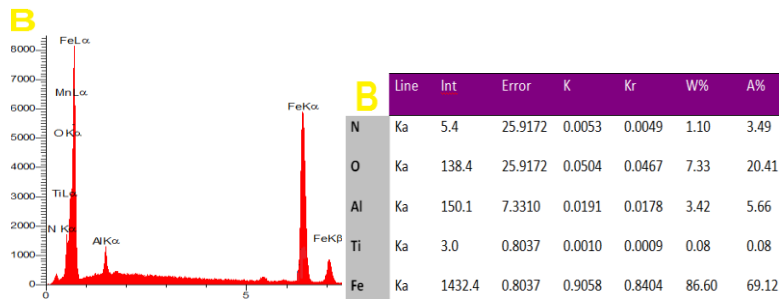
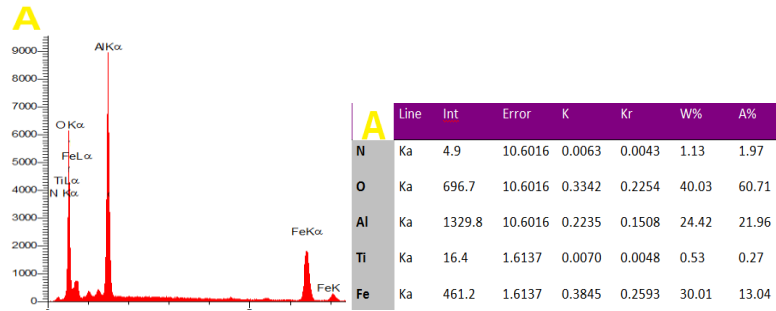
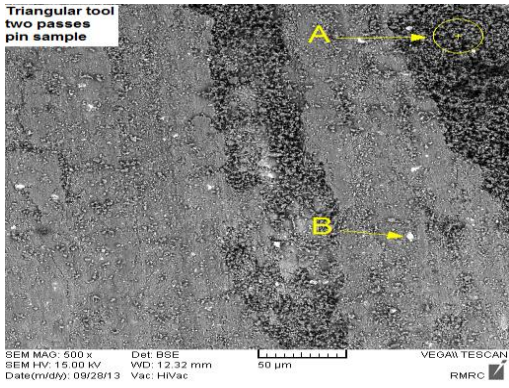


Figure 4.18 The EDS analysis of pin surface

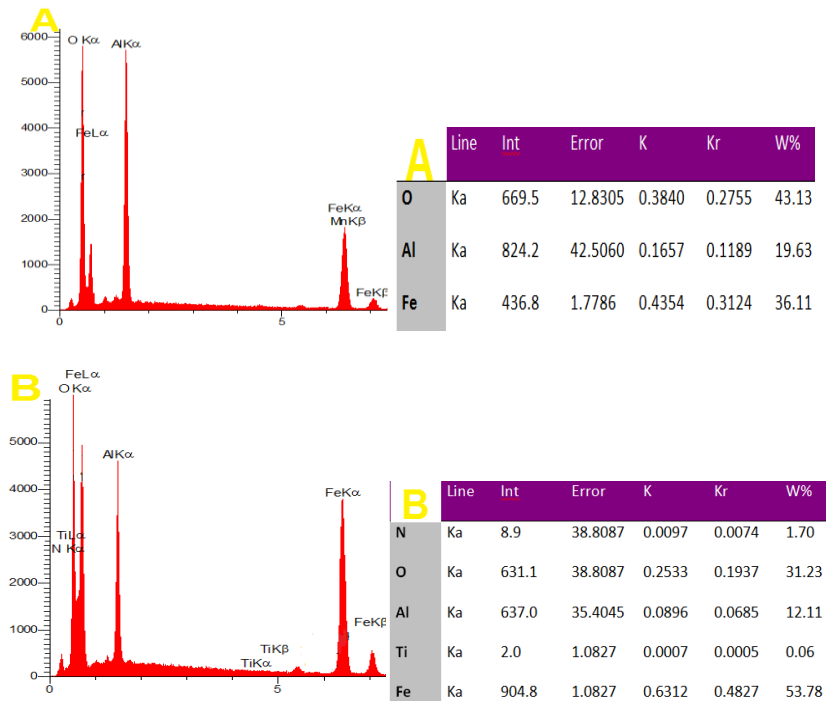
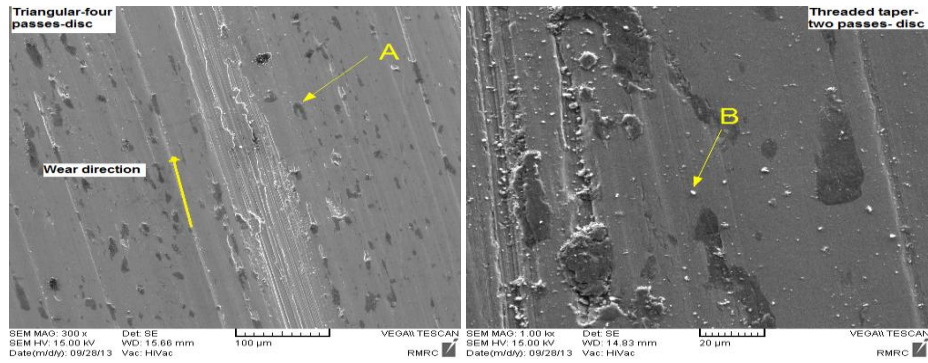


Figure 4.19 The EDS analysis of disc wear surface

Figure 4.20, (A) and (B) shows the SEM picture of pin wear surface of the wear tracks of AL 7075. The abrasion that occurs during the wear process is recognizable by generated grooves inside the wear trails (A); also the adhesive wear phenomena can be understood by the material trace removal (B).

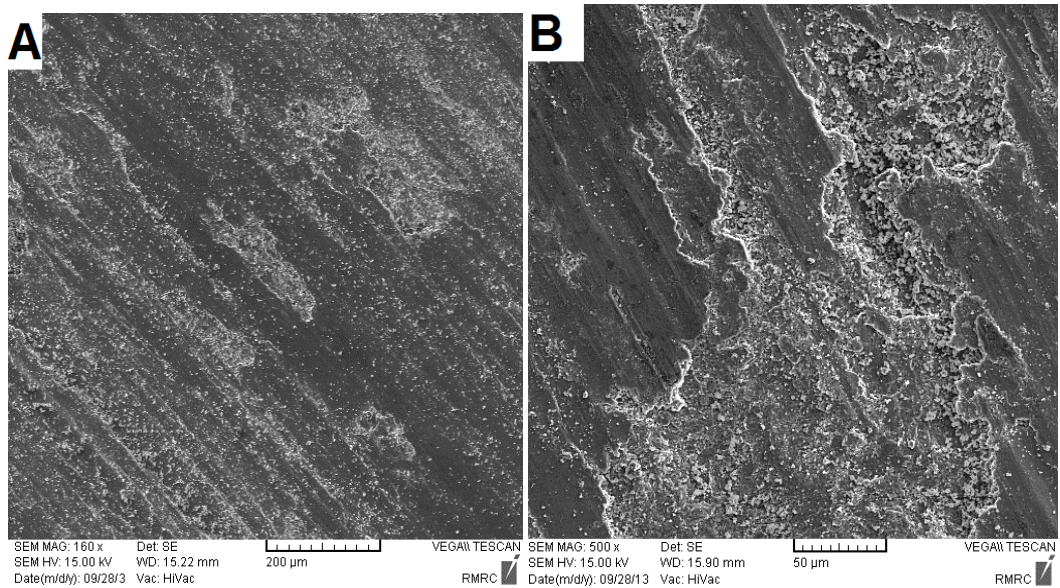


Figure 4.20 SEM picture of wear surface

4.7.2 Effect of FSP on Micro hardness

In friction stir processing, the important effective parameters on hardness are (1) grain size (2) hard secondary phase sediments and (3) Orowan strengthening due to good distribution of reinforcement particles.

Figure 4.21 shows the hardness of FSP samples which are produced by different tool shapes and pass number. It is clear that by approaching the weld zone in all samples the hardness increase which occurs due to a reduction in grain size after FSP and TiN nano-powder distribution in base material is seen as a main reason. The hardness mapping in some results is non-uniform. The reason is non-homogenous distribution of nano-powder; in some regions where there is a high density of nano-powder the hardness elevates and in regions where the nano-powder density is lower the hardness is reduced, additionally high density of nano-powder also can stop the grain growth and, as a result higher grain size reduction. Higher temperature in SZ reduces the dislocation congestion which worsen the hardness [37]

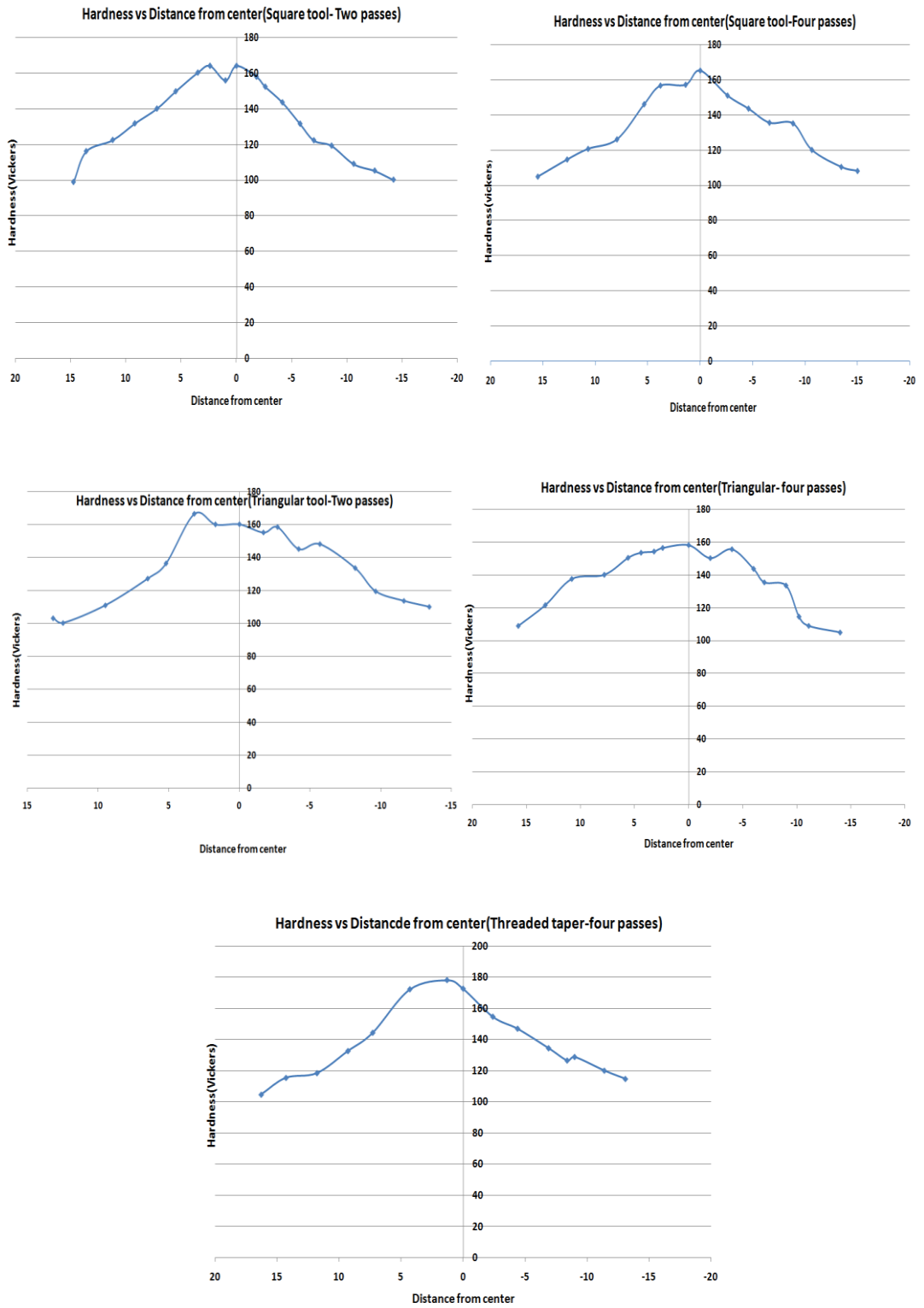


Figure 4.21 Hardness distribution VS distance from weld center

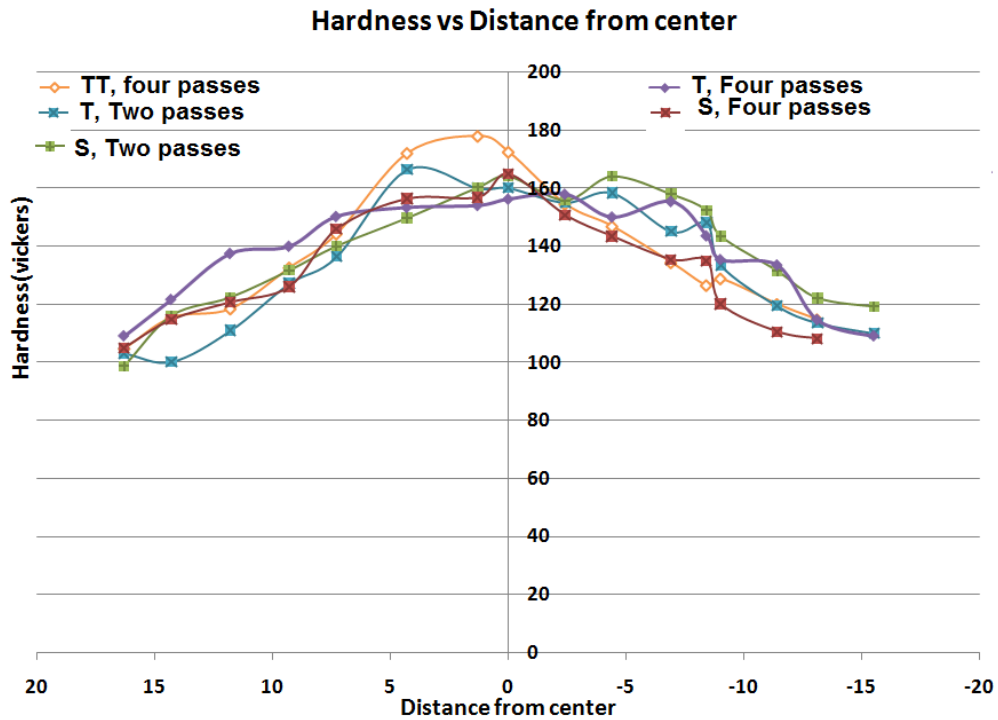


Figure 4.21 Hardness distribution VS distance from weld center

Figure 4.22 shows the Mean Hardness of samples, the best value belongs to threaded taper tool. The second best value belongs to Triangular tool, this value increases with an increase in the pass number. The lowest value belongs to the square tool. These results are completely matched with obtained result about grain size and pass number, which show the finest grain size samples approach the better hardness properties and good nano-powder distribution has the same effect on hardness properties.

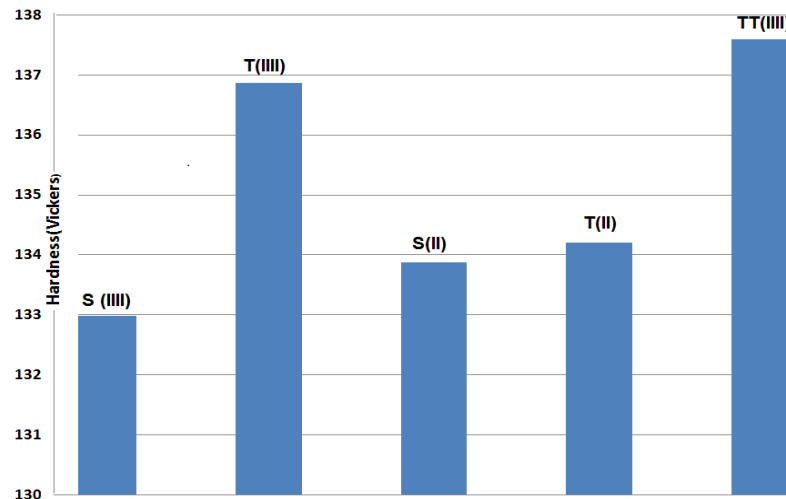


Figure 4.22 The average hardness of samples

4.7.3 Effect of the FSP Process on the Tensile Properties of Material

Tensile traits are based on some parameters such as, grain size, content of dislocations and porosity, content of accumulative reinforcement powder in SZ and state of combination (bounding) between parent material and reinforcement powder [36].

After running tensile test on specimens, the specimen fracture at specific value of time, force and displacement data are used to calculate the stress, strain, and elongation percent. Figure 4.23 shows the tensile samples after fracture.

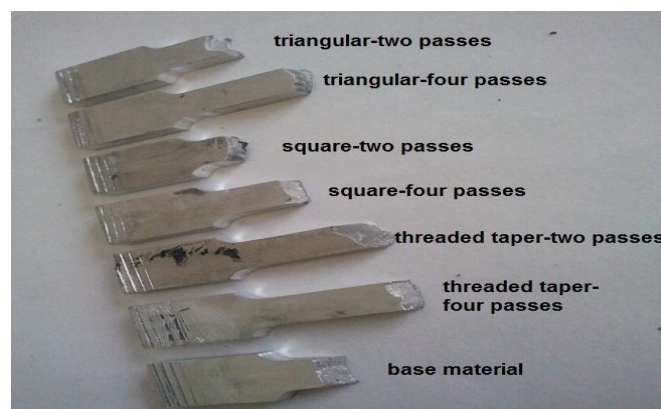


Figure 4.23 Tensile samples after fracture

Table 4.3 lists the mechanical properties of base material and FSP samples. Analyzing the data on the table shows that the best values (tensile strength and elongation) belong to the square tool four passes followed by the threaded taper tool two passes.

Table 4.3 the mechanical properties of FSP samples.

Tool shape (Pass number)	T(2)	T(4)	S(2)	S(4)	TT(2)	TT(4)	Base
(UTS)	382.97 (66.14%)	276.28 (47.7%)	342.72 (59.2%)	454.25 (78.2%)	426.26 (73.6%)	397.33 (68.6%)	579
Elongation (%)	5.8%	5.4%	6.88%	8.38%	9.6%	7.52%	10.8 %

Chapter 5

CONCLUSION

In this research, a TiN-AL7075 nano-composite was formed through employing a novel thermo-mechanical alloying technique called as Friction Stir Processing. The effect of variation in tool geometry and tool-rotation direction was investigated on the distribution of nano-powder. The composite was characterized through various mechanical and microstructural techniques. The following important findings can be drawn from the study:

1. Nano-powder is scattered with varying degree of density in the FSP zone, which can be viewed as bright and dark region in SEM micrographs with former indicating high density of nano-powder and black low density of nano powder.
2. The shape of tool affects the grain refinement. The best refinement is offered by threaded taper tool (MGS: 1.4 μ m) followed by triangular tool (MGS: 1.086) and square tool (MGS: 2.4 μ m)
3. The number of passes affects size of grain in composite. Employing threaded tool, with 2 passes 30 times and with 4 passes 50 times grain reduction has been recorded.
4. Density of nano powder play an important role in the grain size, SEM mapping picture of nano-powder distribution shows that in regions with high density of nano-powder the grain growth restricted because of these particles pinning.
5. Changing the tool rotation direction causes to homogeneous material flow pattern in advancing side and retreating side of SZ.

6. The SEM mapping picture of nano powder distribution in advancing and retreating side of FSP zone shows the good nano-powder distribution. The best distribution occurs in threaded taper followed by triangular tool and then followed by square tool. The same fact endorsed by SEM analysis.
7. The XRD analysis of the FSP zone provides evidence of creation of new intermetallic material phases. The maximum number of phases(4) are achieved with square followed by the triangular tool(3). This can be reasoned by the fact that square tool causes more turbulence and heat generation than triangular tool. By increasing the number of passes, intermetallic phases have been found to be increasing further.
9. The XRD analysis of the FSP zone provides evidence of creation of new intermetallic material phases).
10. The FSP with TiN powder has demonstrated capability to improve wear resistance of 7075AL compared with based material. This, as revealed from the EDS analysis of the pins and discs surface, is because of a fact that ferric oxide and TiN element produced on the surfaces which significantly reduced wear. The wear performance of nano-composite has been found to be affected by number of passes besides shape of tool. Thread taper tool has appeared as the best tool followed by square tool; While, wear performance increase with increasing number of passes.
11. The FSP has showed increase in micro-hardness of the base material in SZ, regardless of the shape of tool. However, thread taper with 4 passes produced the best results.
13. Overall tensile properties (tensile strength and elongation) of nano-composite have been observed to be reduced slightly compared with base material. This can most probably be attributed to the role of TiN.

REFERENCES

- [1] Threadgill, P.L., Leonard, A.J., Shercliff, H.R., Withers, P.J., 2009. Friction stir welding.
- [2] Mark Easton, Wei Qian Song, Trevor Abbott, “A comparison of the deformation of magnesium alloys with aluminium and steel in tension, bending and buckling”, *Materials and Design* 27 (2006) 935–946.
- [3]Mohammd Reza Firouzmanesh, “ composite materials with theory of new thermal analysis methods ”.
- [4] Reza Abdie“study of material and processes parameters effect in friction stir welding of dissimilar aluminium alloys”. Master Thesis.
- [5] R.S. Mishra , Z.Y. Ma, I. Charit, “Friction stir welding and processing”, *Materials Science and Engineering R* 50 (2005) 1–78
- [6]B.M. Darras, M.K. Khraisheh, F.K. Abu-Farha, M.A. Omar, “Friction stir processing of commercial AZ31 magnesium alloy”, *Journal of Materials Processing Technology* 191 (2007) 77–81
- [7] R.S. Mishra, Z.Y. Ma, I. Charit, “Friction stir processing: a novel technique for fabrication of surface composite”, *Materials Science and Engineering A*341 (2003) 307-310.

- [8] Douglas C. Hofmann, Kenneth S. Vecchio, “Submerged friction stir processing (SFSP): An improved method for creating ultra-fine-grained bulk materials”, *Materials Science & Engineering A* 402 (2005) 234–241
- [9] K. Elangovan, V. Balasubramanian, “Influences of tool pin profile and axial force on the formation of friction stir processing zone in AA6061 aluminium alloy”, *IntJ AdvManufTechnol* 38 (2008) 285–295.
- [10] Saad Ahmed Khodir, Toshiya Shibayanagi, “Friction stir welding of dissimilar AA2024 and AA7075 aluminium alloys”, *Materials Science and Engineering B* 148 (2008) 82–87.
- [11] P. Cavaliere, E. Cerri, “Mechanical response of 2024-7075 aluminium alloys joined by Friction Stir Welding”, *JOURNAL OF MATERIALS SCIENCE* 40 (2005) 3669 – 3676.
- [12] R.S. Mishra, M.W. Mahoney, S.X. McFadden, N.A. Mara, A.K. Mukherjee, *Scripta Mater* 42 (2000) 163.
- [13] R.S. Mishra, M.W. Mahoney, *Mater. Sci. Forum* 507 (2001) 357–359.
- [14] Z.Y. Ma, R.S. Mishra, M.W. Mahoney, *Acta Mater.* 50 (2002) 4419.
- [15] R.S. Mishra, Z.Y. Ma, I. Charit, *Mater. Sci. Eng. A* 341 (2002) 307.

- [16] Z. Y. Ma, S.R. Sharma, R.S. Mishra, M.W. Manohey, Mater.Sci.Forum 426–432 (2003) 2891.
- [17] C.J. Hsu, C.Y. Chang, P.W. Kao, N.J. Ho, C.P. Chang, “Al–Al₃Ti nanocomposites produced in situ by friction stir processing”, Acta Materialia 54 (2006) 5241–5249.
- [18] A. Shafiei-Zarghani, S.F. Kashani-Bozorg, A. Zarei-Hanzaki, “Microstructures and mechanical properties of Al/Al₂O₃ surface nano-composite layer produced by friction stir processing”, Materials Science and Engineering A 500 (2009) 84–91.
- [19] F.C. Liu, Z.Y. Ma, “Low-temperature superplasticity of friction stir processed Al–Zn–Mg–Cu alloy”, Scripta Materialia 58 (2008) 667–670.
- [20] D.K. Lim, T. Shibayanagi, A.P. Gerlich, “Synthesis of multi-walled CNT reinforced aluminium alloy composite via friction stir processing”, Materials Science and Engineering A 507 (2009) 194–199.
- [21] K. Elangovan, V. Balasubramanian, “Influences of tool pin profile and tool shoulder diameter on the formation of friction stir processing zone in AA6061 aluminium alloy”, Materials and Design 29 (2008) 362–373.
- [22] P. Cavaliere, P.P. De Marco, “Fatigue behaviour of friction stir processed AZ91 magnesium alloy produced by high pressure die casting”, Materials Characterization 58 (2007) 226–232.

- [23] L. Commin, M.D., J.E. Masse, L. Barrallier, “Friction stir welding of AZ31 magnesium alloy rolled sheets: Influence of processing parameters”. *Acta Materialia* 59 (2009) 326–334. H. Zhang, S.B. Lin, L. Wu, J.C. Feng, Sh.L. Ma, “Defects formation procedure and mathematic
- [24] Model for defect free friction stir welding of magnesium alloy”, *Materials and Design* 27 (2006) 805–809..
- [25] A. Kostka, R.S. Coelho, J. dos Santosb, A.R. Pyzalla, “Microstructure of friction stir welding of aluminium alloy to magnesium alloy”, *Scripta Materialia* 60 (2009) 953–956.
- [26] Z.Y. Ma, A.L. Pilchak, M.C. Juhas, J.C. Williams, “Microstructural refinement and property enhancement of cast light alloys via friction stir processing”, *Scripta Materialia* 58 (2008) 361–366.
- [27] Y. S. Sato, S. H. C. Park, A. Matsunaga, A. Honda, H. Kokawa, “Novel production for highly formable Mg alloy plate”, *Journal of Materials Science* 40 (2005) 637– 642.
- [28] J.W. Martin, R.D. Doherty, “Stability of Microstructures in Metallic Systems”, Cambridge University Press, Cambridge, 1976. 28.
- [29] Fei-Yi Hung, Chien-Chih Shih, Li-Hui Chen, Truan-Sheng Lui, “Microstructures and hightemperature mechanical properties of friction stirred AZ31–Mg alloy”, *Journal of Alloys and Compounds*, 428 (2007) 106–114.

- [30] L.E. Murr, G. Liu, J.C. McClure, *J. Mater. Sci.* 33 (1998) 1243.
- [31] W. Tang, X. Guo, J.C. McClure, L.E. Murr, *J. Mater. Process. Manufact. Sci.* 7 (1998) 163.
- [32] P. Cavaliere, P.P. De Marco, “Fatigue behaviour of friction stir processed AZ91 magnesium alloy produced by high pressure die casting”, *Materials Characterization*, 58 (2007) 226–232.
- [33] Y. Morisada, H. Fujii, T. Nagaoka, M. Fukusumi, “Effect of friction stir processing with SiC particles on microstructure and hardness of AZ31”, *Materials Science and Engineering A* 433 (2006) 50–54.
- [34] C.I. Chang, X.H. Du, J.C. Huang, “Producing nanogained microstructure in Mg–Al–Zn alloy by two-step friction stir processing” *Scripta Materialia*, 59 (2008) 356–359.
- [35] A.H. Feng, Z.Y. Ma, “Enhanced mechanical properties of Mg–Al–Zn cast alloy via friction stir processing”, *Scripta Materialia* 56 (2007) 397–400.
- [36] Barmouz M, BesharatiGivi MK, Seyfi J. On the role of processing parameters in producing Cu/SiC metal matrix composites via friction stir processing : Investigating microstructure, microhardness, wear and tensile behavior. *Materials characterization* 2011;62:108–17.

- [37]Zahmatkesh B, Enayati MH. A novel approach for development of surface nanocomposite by friction stir processing. Mater SciEng: A 2010;527(24–25):6734–40
- [38]R.S. Mishra and Z.Y. Ma, “Friction stir welding and processing”. Materials Science and Engineering R, Vol. 50 (2005), p. 1-78.
- [39] R. Nandan, T. DebRoy, H.K.D.H Bhadeshia. “Recent advances in friction-stir welding – Process, weldment structure and properties”, Progress in Materials Science, Vol 53 (2008), p. 980-1023